



Lattice Boltzmann method for heat transfer in phase change materials: a review

Sudhanshu Kumar¹ · Debabrata Panda¹ · Praveen Ghodke² · Krunal M. Gangawane¹

Received: 21 September 2022 / Accepted: 28 January 2023 / Published online: 28 February 2023
© Akadémiai Kiadó, Budapest, Hungary 2023

Abstract

Over the years, incredible evolution has been framed in developing particle-induced discrete simulation techniques over conventional continuum approaches. In particular, the lattice Boltzmann method (LBM) originated from a flexible and robust computational tool for scientific research and various practical applications. LBM is based on a mesoscopic approach that acts as a bridge between the microscale and macroscale, offering distinct features in the accuracy of simulations and numerical efficiency. LBM has been successfully employed over a broad aspect of disciplines, encompassing biomedicine, geothermal energy, flow physics, materials, chemistry, medical treatment, storage of energy, and several engineering disciplines. Meanwhile, phase change materials (PCMs) are extensively utilized in thermal energy storage (TES) systems as they can absorb and release heat throughout the phase change process. Moreover, phase change heat transfer (HT) has a substantial occurrence in industrial and domestic activities. It is expected to enhance the thermal transport rate between HT fluid and PCMs for the confinement of a larger amount of heat. This current work aims to provide a comprehensive review of LBM for thermo-fluids concentrating on thermal flows and PCM. It also enlightens a brief insight into the LBM formulation of heat transfer for PCMs under various external force conditions and the implementation of boundary conditions for PCMs. In addition, it also introduces the study and examination of the existing TES systems comprising PCMs for various applications.

Keywords Phase change materials · Lattice Boltzmann method · Thermal energy storage · Heat transfer

Abbreviations

AR Aspect ratio of enclosure/cavity, dimensionless
Da Darcy number, dimensionless
 F External force, N
Ma Mach number
 ε Porosity
 f_l Volume fraction of liquid
 p Distribution function for flow field
 \underline{g} Gravitational acceleration ($m\ s^{-2}$)
 \overline{Nu} Average Nusselt number, dimensionless
Nu Local Nusselt number, dimensionless
 q Distribution function for thermal field
 C Specific heat at constant pressure $kJ\ kg^{-1}\ ^\circ C^{-1}$
 c_i Discrete lattice speed in an i th direction ($m\ s^{-1}$)
 ΔH Latent enthalpy ($kJ\ kg^{-1}$)

Δt Time step (s)
 w_i Mass function in the particular direction
Ra Rayleigh number, dimensionless
Re Reynolds number, dimensionless
 H Total enthalpy ($kJ\ kg^{-1}$)
 H_l Total enthalpy liquidus temperature ($kJ\ kg^{-1}$)
 H_s Total enthalpy solidus temperature ($kJ\ kg^{-1}$)
 T Temperature, K
 M Nodal number
 n Power-law index, dimensionless
 x, y Cartesian coordinates, m
 t Time, sec
 T_m Melting temperature
 L Latent heat of melt ($kJ\ kg^{-1}$)
 \mathbf{u} Velocity, $m\ s^{-1}$
 θ Dimensionless temperature,
 U Dimensionless velocity
 P Dimensionless pressure
Pr Prandtl number
 φ Volume fraction of nanoparticle
St Stefan number
 F_o Fourier number

✉ Krunal M. Gangawane
gangawanek@nitrrkl.ac.in

¹ Department of Chemical Engineering, National Institute of Technology Rourkela, Odisha 769008, India

² Department of Chemical Engineering, National Institute of Technology Calicut, Calicut 673601, India

β_T	Thermal expansion coefficient, K^{-1}
ω	Collision frequency
ρ	Density of the fluid, $kg\ m^{-3}$
ν	Kinematic viscosity, $m^2\ s^{-1}$
α	Thermal diffusivity, $m^2\ s^{-1}$
Ω	Collision operator
τ	Relaxation factor
ω_p	Collision frequency for flow
ω_q	Collision frequency for temperature

Introduction

Over the decades, the energy demand has increased dramatically due to rapid population and economic growth. The emerging tremendous energy utilization leads to the enormous emission of CO_2 (carbon dioxide) and yields harmful contents, leading to environmental pollution and global warming [1–3]. Phase change materials (PCMs) are endorsed as one of the potential thermal energy storage (TES) media that have been experiencing noteworthy interest over the globe [4–6]. Several techniques have flourished and enhanced thermal applications to preserve energy costs to treat these disasters. The TES system is a valuable tool for increasing energy efficiency to fill the disparity between energy demand and furnishing [7]. In general, TES systems are categorized as sensible heat thermal energy storage (SHTES) and other one is latent heat thermal energy storage (LHTES) systems. LHTES employs PCMs to accumulate energy and allows the systems to adopt and liberate a tremendous amount of heat energy with a thermal variation by the phase change process (PCP) of PCMs. It provides a large amount of heat storage density and can potentially preserve high heat as latent heat (LH) of fusion with a little number of PCMs and a moderate thermal variation [8–10]. However, the lower thermal conductivity of PCMs used in the LHTES system reduces thermal energy [11]. Heat transfer in PCMs has been considered an attractive research scope in thermal science. There are several approaches to enhance the thermal capability of PCM, i.e., the use of porous foams, miniature heat pipes, dispersion of nanoadditives with higher thermal conductivity in PCM, and micro- and macroencapsulation. The most feasible and economical strategy to enhance the thermal capacity of PCMs is the dispersion of high thermal conductivity nanoadditives in PCM (NePCM) [12, 13]. PCMs have become an alternative for thermal management owing to chemical steadiness, cheap rate, and large energy density. Energy and combustion systems usually embrace hydrodynamics, thermal transport, chemical reactions, and phase change (PC) over scales varying from macroscale to microscale via mesoscale. The studies related to PCMs are of substantial significance in several engineering and natural systems. It includes metal smelting and casting, Li-ion

batteries, solar thermal energy storage, air-conditioning unit, refrigeration system, electronic cooling, drug delivery unit, crystal growth, TES in buildings, TES, welding, alloys, and metallurgical process [14–22]. The matter is exposed to a solid–liquid PCP. The number of research publications on heat transfer for PCMs by LBM has seen significant growth over the last ten years, as illustrated in Fig. 1.

Consequently, the moving interface separates two distinct phases and evolves the absorption or release of LH in the vicinity of the interface. Mathematical modeling of such a system is considered one of the challenging tasks due to complex boundary treatment and variations of the thermo-physical properties. Over the last three decades, LBM has been extensively acknowledged and used to numerically investigate challenging problems due to its advantage in the mesoscopic background and easy execution of boundary conditions in parallel computing. Theoretical, experimental, and numerical studies have yielded broad literature on different aspects of the PC study, encompassing fundamental studies of the PC phenomenon [2, 24], material features [25, 26], experimental techniques, thermal transport augmentation [3, 27–29], mathematical modeling, and numerical methods [30–32]. In contrast, the numerical simulation technique is a primary course of action due to its higher economy and efficiency, which significantly develops the understanding of melting and solidification processes in the TES system. Some of the familiar methods utilized to analyze the melting and solidification models so far as the finite element method (FEM) [33], finite difference method (FDM) [34], finite volume method (FVM) [35–37], and LBM [38, 39]. PCMs have extensive applications in various industries, including telecommunications, satellites, textiles, medicine, submarine equipment, and transportation, given their phase

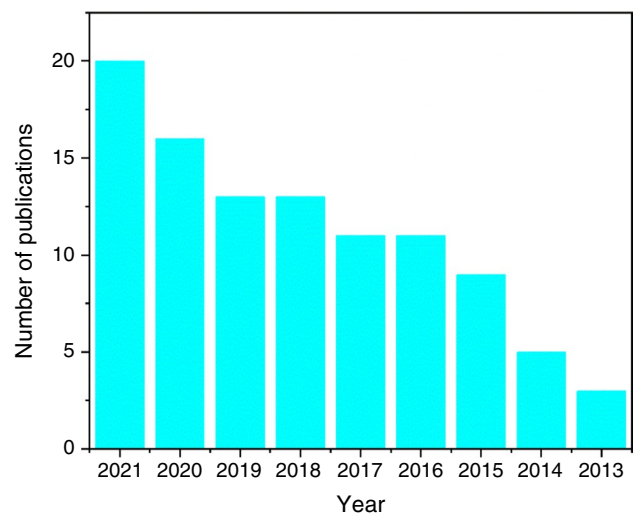
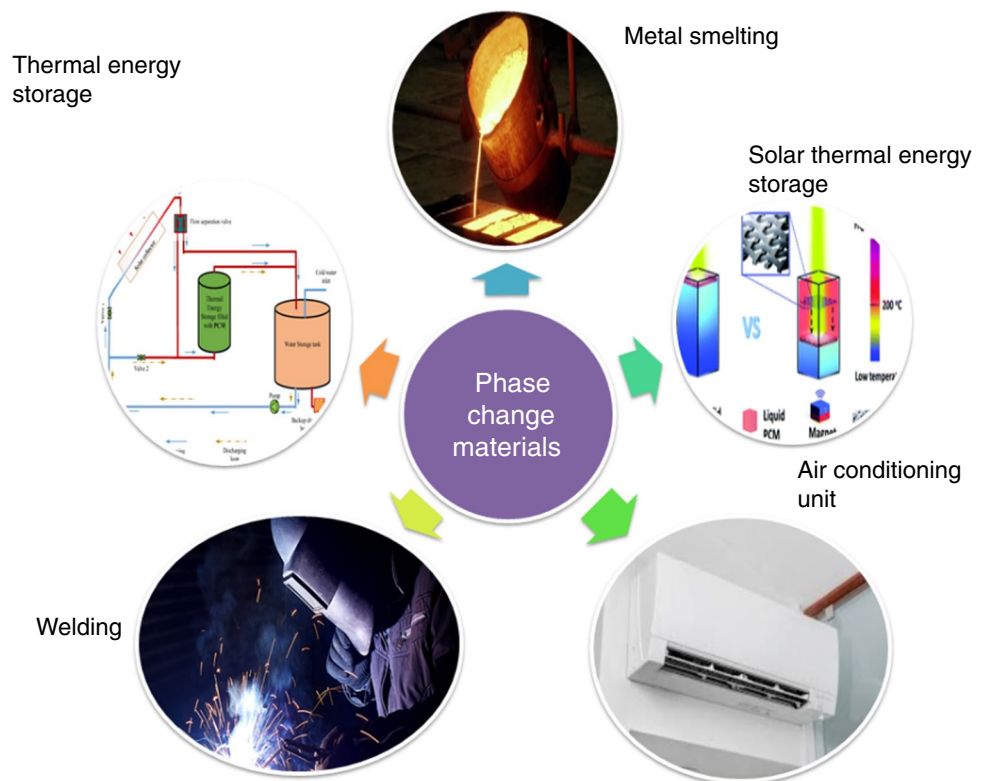


Fig. 1 Research articles published on PCM by LBM [23]

Fig. 2 Application span of PCMs [14–22]



change temperatures [40], as some of the applications are depicted in Fig. 2.

PCMs for thermal energy storage

PCMs are used to store thermal energy, as SHTES and LHTES are among the significant classes of modern materials that largely impart to the efficient use and preservation of solar energy and waste heat [41–43]. Nowadays, TES is recognized as a promising technology to encounter upcoming energy demand. TES is based on PCMs as an energy storage medium due to their cheap rate, easy availability, and high storage capacity [44]. Over the globe, researchers are investigating TES, especially PCM, for their significant benefits in assisting thermal comfort in houses or buildings, improving energy efficiency, and lending to the diminution of environmental pollution [45].

TES can be attained by heating, melting, solidifying, cooling, or vaporizing a material with the energy obtainable as heat when the process is reversed. PCM is the potential medium for TES owing to its extensive latent heat value (140–970 kJ/Kg) [46]. TES systems can potentially boost the effective exercise of thermal energy gadgets and assist in large-scale fuel substitution [47, 48]. For effective utilization of the TES system, PCM and HT mechanism selection plays a significant role [49]. HT augmentation in LHTES systems is attained by either geometric arrangement or thermal conductivity augmentation, and the usage

of extended surfaces like fins (triangular, conical, square, and rectangular fins) or heat pipes is one of the standard techniques for thermal transport augmentation in LHTES systems [50, 51]. The suitable design of TES systems utilizing PCMs needs quantitative information about the PCM's HT and PCP. In Korea, radiant surface heating systems, conventionally worn in residential houses, have about 57% of the residential building energy utilization in heating [52]. The application of PCMs for solar TES capacities has obtained attention due to their vast storage capability and the isothermal nature of the storage technique [53]. PCM-TES has a potent energy-saving solution in air-conditioning applications [54].

Moreover, the applications of PCMs in diverse fields include thermal therapy of the human body, the thermal management of electronic devices, and flexible sensors [55]. Nanoencapsulated PCMs are considered one of the possible materials for TES [56, 57]. The application of organic PCMs can be used for TES systems such as biomass of maize straw and wood; synthesis of core-shell paraffin silica nanocomposite is used as PCM [58–62]. TES system is extensively utilized in waste heat recovery and consumption, building heating, air conditioning, solar thermal power plants, and compressed air energy storage [63–66]. The carbon-based nanostructures (CNs) with higher thermal conductivity can be considered for PCM to improve the thermal properties of the attained

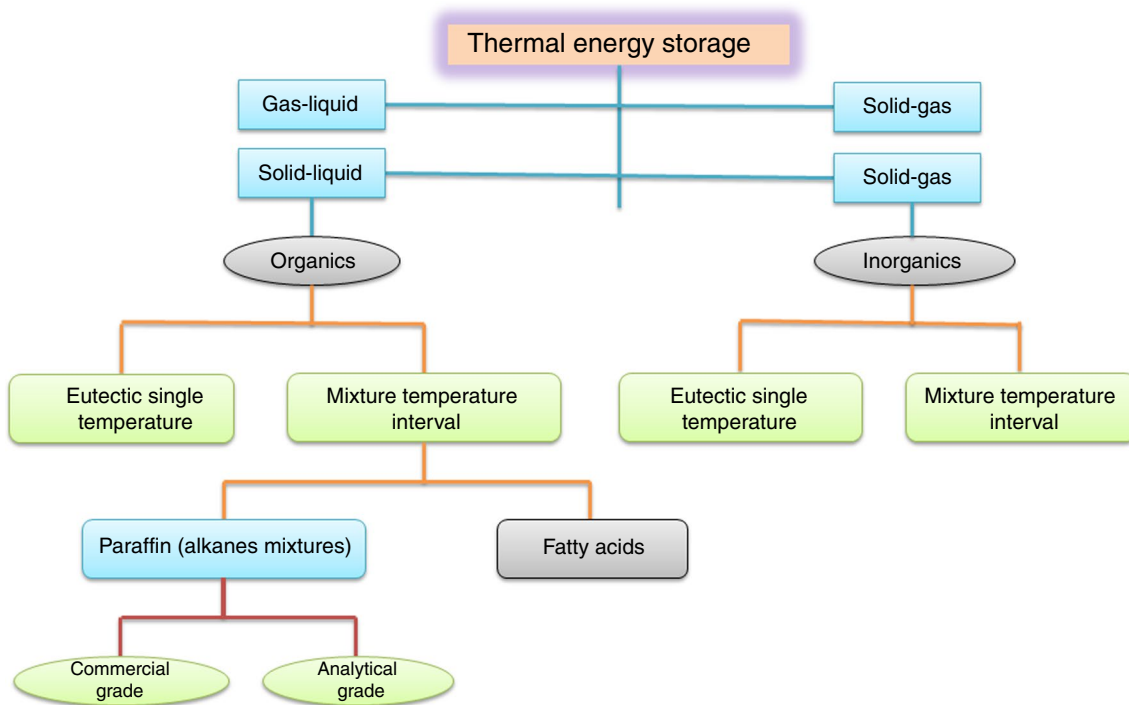


Fig. 3 Classification of PCMs [47, 48]

nanocomposites [67, 68]. The classification of PCMs for TES is exemplified in Fig. 3.

Governing equations

The governing equation of heat transfer for PCMs includes continuity, momentum, and energy equation, which are illustrated below in dimensional form [69–71]

$$\frac{\partial \rho}{\partial t} + \nabla \cdot (\rho \mathbf{u}) = 0 \tag{1}$$

$$\frac{\partial(\rho \mathbf{u})}{\partial t} + \nabla \cdot (\rho \mathbf{u} \mathbf{u}) = -\nabla p + \nabla \cdot (\mu \nabla \mathbf{u}) + \rho F \tag{2}$$

$$\frac{\partial T}{\partial t} + \nabla \cdot (\mathbf{u} T) = \alpha \nabla^2 T + q \tag{3}$$

$$F = g \beta_T (T - T_0) \tag{4}$$

where g , ρ , p , \mathbf{u} , μ , and T are the acceleration due to gravity, density, pressure, velocity, dynamic viscosity, and temperature, respectively. F symbolizes body force, and q stands for heat source term, which occurs through absorption or liberation of LH and is expressed as:

$$q = \left[\frac{\partial(\rho \Delta H)}{\partial t} + \nabla \cdot (\rho \mathbf{u} \Delta H) \right] \tag{5}$$

In the above equation ΔH , the latent enthalpy of the computational cell experiences a PC, and if the material is pure, the second term can be ignored. So, q can become

$$q = -\frac{\partial(\rho \Delta H)}{\partial t} = -\frac{\partial(\rho L f_l)}{\partial t} \tag{6}$$

where L symbolizes the LH of melt and f_l is a fraction of liquid, which can be determined as

$$f_l = \frac{\Delta H}{L} \tag{7}$$

Non-dimensional form

$$\frac{\partial \rho}{\partial t^*} + \nabla \cdot (\mathbf{U}) = 0 \tag{8}$$

$$\frac{\partial \mathbf{U}}{\partial t^*} + \nabla \cdot (\mathbf{U} \mathbf{U}) = -\nabla P + \text{Pr} \nabla^2 \mathbf{U} + \text{Pr} \text{Ra} \theta \tag{9}$$

$$\frac{\partial \theta}{\partial t^*} + \nabla \cdot (\mathbf{U} \theta) = \nabla^2 \theta - \frac{1}{\text{St}} \frac{\partial f_l}{\partial t} \tag{10}$$

The subsequent scaling parameters are utilized to acquire non-dimensional variables

$$\begin{aligned} X &= \frac{x}{L}, Y = \frac{y}{L}, U = \frac{uL}{\alpha}, t^* = \frac{t\alpha}{L^2}, \\ P &= \frac{p}{\rho\alpha^2}, \theta = \frac{T - T_C}{T_h - T_C} \end{aligned} \tag{11}$$

After exploring the general macroscopic governing equations of phase change materials for heat transfer, let us briefly look at the mesoscopic technique, i.e., LBM.

Lattice Boltzmann method

LBM has gained massive impetus in science and technology as the potential tool for solving various engineering applications. Namara and Zanetti (1988) introduced to beat the imperfections of lattice gas cellular automata (LGCA) [72]. It is a new technique in computational fluid dynamics (CFD). It is a mesoscopic scheme and is prominent among the recent simulation schemes established on the molecular hypothesis in CFD. It is established on the Boltzmann equation (BE), governed by the kinetic theory of gases [73]. These models incorporate essential physics [74, 75]. In LBM, the flow particles are replaced by distribution functions (DFs) of the fractious particles. LBM's evolution occurs through streaming and collision [73, 76–80]. With the Bhatnagar–Gross–Krook (BGK) collision model, LBM has developed astonishing advances in solving various problems associated with fluid flow. It is one of the most proficient pseudo-kinetic algorithms. The LBM approach solves several problems associated with fluid flow, thermal, species transport, multiphase, and heat transfer for phase change material (PCM). LBM has several advantages, such as coherent in the algorithm, proficiency in treating complicated geometrics, easy execution of boundary treatment, eminent accuracy, easiness in parallel computing, improved stability, modified pressure estimation, and robustness for non-trivial geometries and complex physical phenomena [81]. A thermal lattice Boltzmann method (TLBM) is utilized to solve the problems based on HT for PCMs [82–85].

A generalized form of the BE can be yielded as [86–88],

$$\frac{\partial p_i}{\partial t} + \mathbf{c} \cdot \nabla p = \Omega \tag{12}$$

where p is the particle distribution function (PDF), t is time, \mathbf{c} is lattice, and Ω is the collision operator, and it is in integrodifferential form, which develops the solution of Eq. (12) complex. A simple approximation proposed by BGK is usually used to overwhelm this problem. It is represented as follows:

$$\Omega = \omega(p^{\text{eq}} - p) = \frac{1}{\tau}(p^{\text{eq}} - p) \tag{13}$$

where ω , p^{eq} , and τ are collision frequency, equilibrium distribution function (EDF), and relaxation factor, respectively.

The BE with BGK approximation can be given as,

$$\frac{\partial p_i}{\partial t} + c_i \nabla p_i = \frac{1}{\tau}(p^{\text{eq}} - p) \tag{14}$$

The discretization of Eq. (14) in space with time yields the lattice Boltzmann equation (LBE), which is introduced as follows [89, 90].

$$p_i(\mathbf{x} + \mathbf{c}_i \Delta t, t + \Delta t) - p_i(\mathbf{x}, t) = -\omega [p_i(\mathbf{x}, t) - p_i^{\text{eq}}(\mathbf{x}, t)] \tag{15}$$

The various symbols in the above equation \mathbf{x} , Δx , i , Δt , c_i , p_i and p_i^{eq} are coordinates, lattice step size, lattice link direction, time step, discrete velocity, PDF, and EDF.

- Collision (RHS of Eq. 15)

$$\bar{p}_i(\mathbf{x}, t) = p_i(\mathbf{x}, t) - \omega [p_i(\mathbf{x}, t) - p_i^{\text{eq}}(\mathbf{x}, t)] \tag{16}$$

- Streaming (LHS of Eq. 15)

$$p_i(\mathbf{x} + \mathbf{c}_i \Delta t, t + \Delta t) = \bar{p}_i(\mathbf{x}, t) \tag{17}$$

LBM for phase change materials

LBM for the PCMs in heat transfer is discussed herein. In general, for the study of the thermal field by LBM, there are three crucial approaches for attaining it, i.e., the multispeed approach [83] double distribution function (DDF) approach [84], and the passive scalar thermal lattice Boltzmann method (PS-TLBM) [91]. In the case of PCM for heat transfer, two distribution functions are utilized: flow field (p) and thermal field (q). LBM formulation for PCM is expressed as

$$p_i(\mathbf{x} + \mathbf{c}_i \Delta t, t + \Delta t) = p_i(\mathbf{x}, t) - \omega_p [f_i(\mathbf{x}, t) - p_i^{\text{eq}}(\mathbf{x}, t)] + \Delta t F_i \tag{18}$$

$$q_i(\mathbf{x} + \mathbf{c}_i \Delta t, t + \Delta t) = q_i(\mathbf{x}, t) - \omega_q [q_i(\mathbf{x}, t) - q_i^{\text{eq}}(\mathbf{x}, t)] \tag{19}$$

where f_i^{eq} and g_i^{eq} are the EDF for flow and thermal fields, respectively, and they can be formulated as below.

$$p_i^{\text{eq}} = w_i \rho(\mathbf{x}, t) \left[1 + \frac{6(\mathbf{u} \cdot \mathbf{c}_i)}{2c_s^2} + \frac{4.5(\mathbf{u} \cdot \mathbf{c}_i)^2}{c_s^4} + \frac{1.5(\mathbf{u} \cdot \mathbf{u})}{c_s^2} \right] \tag{20}$$

$$q_i^{eq} = w_i T(\mathbf{x}, t) \left[1 + \frac{3(\mathbf{c}_i \cdot \mathbf{u})}{c_s^2} \right] \tag{21}$$

where \mathbf{u} , ρ , \mathbf{c}_i , and w_i represents the macroscopic variables velocity, density, lattice link velocity, and mass function, respectively. The mass function (w_i) for the D2Q9 model (which is mainly the preferred lattice arrangement) and lattice velocity (c_i) can be written as,

$$w_i = \begin{cases} 4/9; & i = 0 \\ 1/9; & i = 1 - 4 \\ 1/36; & i = 5 - 8 \end{cases} \tag{22}$$

$$\mathbf{c}_i = \begin{cases} (0, 0) & ; i = 0 \\ c([\cos(i-1)\pi/2], [\sin(i-1)\pi/2]) & ; i = 1 - 4 \\ c\sqrt{2}([\cos((i-5)\pi/2 + \pi/4)], [\sin((i-5)\pi/2 + \pi/4)]) & ; i = 5 - 8 \end{cases} \tag{23}$$

The parameter collision frequency (ω) is a function of kinematic viscosity and thermal diffusivity; for example, collision frequency for flow and thermal are ω_f and ω_g , respectively. These are expressed as,

$$\omega_p = \frac{1}{3\nu + 0.5} \tag{24}$$

$$\omega_q = \frac{1}{3\alpha + 0.5} \tag{25}$$

The fundamental hydrodynamic and macroscopic quantities such as density (ρ), velocity (\mathbf{u}), and temperature (T) can be computed from the distribution by using the following equations

$$\rho(\mathbf{x}, t) = \sum_i p_i(\mathbf{x}, t) \tag{26}$$

$$\mathbf{u}(\mathbf{x}, t) = \sum_i \frac{p_i(\mathbf{x}, t)c_i}{\rho} \tag{27}$$

$$T = \sum_i q_i(\mathbf{x}, t) \tag{28}$$

The term ' F_i ' is the term [92–95].

$$F_i = w_i F \frac{c_i}{e_s^2} \tag{29}$$

where $e_s = 1/\sqrt{3}$

LBM for solid–liquid PC-based study on thermal LB model was suggested by shan [82]. By modifying the EDF

of the thermal field, a recent approach can be evolved to address the LH source term. Later, Jiaung et al. [96] introduced a simplified energy model called the enthalpy-based model. The enthalpy-based method can be used for solid–liquid PC problems as it eliminates the requirements of meeting conditions at the interface position [71, 96, 97]. The total enthalpy (H) splits into sensible and LH enthalpy components in the vicinity of the solid–liquid interface (SLI) for PCM problems. The total enthalpy can be evaluated by Eq. (31).

$$H = CT(\mathbf{x}, t) + f_1 L(\mathbf{x}, t - \Delta t) \tag{30}$$

$$H = \sum_{i=0}^{n-1} q_i \tag{31}$$

The temperature can be estimated by the total enthalpy as follows [98, 99]

$$T = \begin{cases} \frac{H}{C}; & T < T_s \\ T_s + \frac{H-H_s}{H_1-H_s}(T_1 - T_s); & T_s \leq T \leq T_1 \\ T_1 + (H - H_1)/C; & T > T_1 \end{cases} \tag{32}$$

T_s and T_1 stand for solidus and liquidus temperatures, respectively ($T_1 \geq T_s$ and equal symbol denotes the PCP at a fixed temperature); and H_1 and H_s are the total enthalpy representing the liquidus and solidus temperatures, respectively.

For the thermal field, the source term will be added to Eq. (19), and later, the thermal DF can be obtained as:

$$q_i(\mathbf{x} + \mathbf{c}_i \Delta t, t + \Delta t) = q_i(\mathbf{x}, t) - \omega_q [g_i(\mathbf{x}, t) - q_i^{eq}(\mathbf{x}, t)] - w_i \frac{L}{C} (f_i(\mathbf{x}, t) - f_i(\mathbf{x}, t - \Delta t)) \tag{33}$$

PCM with porous media

For the PCMs in porous media, the external force exercised by the porous medium on the fluid is considered. The expression is given by [100–102]

$$F = -\frac{\epsilon\nu}{K} U - \frac{\epsilon c_F}{\sqrt{K}} |U|U + \epsilon G \tag{34}$$

where ν , K , and c_F are the kinematic viscosity, permeability, and dimensionless Forchheimer term, respectively ($c_F = 1.75/150\epsilon^3$) stated by Fu et al. [103] $|U| = \sqrt{u^2 + v^2}$. The permeability (K) can be computed from Kozeny–Carman equation [104] $K = \epsilon^3 d_p^2 / 150(1 - \epsilon^2)$, where d_p is the mean diameter of pores of the porous medium. The first and second expressions on the RHS (right-hand side) in Eq. (34)

stand for Darcy term and Forchheimer drag forces, respectively, amid a fluid and porous structure applied to describe the essence of the porous media to the fluid flow within the liquid regime. The third expression on the RHS in Eq. (34) symbolizes the buoyancy term in which the Boussinesq approximation is utilized; so, it is given by

$$G = g\beta_f(T - T_0) \tag{35}$$

where g is acceleration owing to gravity, β represents the thermal expansion coefficient, which expresses variations in the volume of the molten PCMs owing to the thermal difference, and T_0 is reference temperature.

LBM for nanoenhanced PCM

It is substantially acknowledged that when the nanoparticles are added to the water or some other working fluid, viscosity, thermal conductivity, and other physical properties will vary. The density of the nanofluid is expressed as [105–107],

$$\rho_{nf} = \rho_f(1 - \phi) + \rho_{sp}\phi \tag{36}$$

$$\mu_{nf} = \frac{\mu_f}{(1 - \phi)^{2.5}} \tag{37}$$

$$(\rho C_p)_{nf} = (\rho C_p)_f(1 - \phi) + (\rho C)_{sp}\phi \tag{38}$$

$$(\rho\beta)_{nf} = (\rho\beta)_f(1 - \phi) + (\rho\beta)_{sp}\phi \tag{39}$$

$$\frac{\sigma_{nf}}{\sigma_f} = 1 + \frac{3\left(\frac{\sigma_{sp}}{\sigma_f} - 1\right)\phi}{\left(\frac{\sigma_{sp}}{\sigma_f} + 2\right) - \left(\frac{\sigma_{sp}}{\sigma_f} - 1\right)\phi} \tag{40}$$

In the above equations ϕ , ρ_{nf} , ρC_{nf} , $\rho\beta_{nf}$, μ_{nf} , and σ_{nf} represent the volume fraction of nanoparticles, density of nanofluid, heat capacity, thermal expansion, dynamic viscosity, and electrical conductivity, and subscripts *nf*, *f*, and *sp* denotes nanofluid, base fluid, and solid particles.

LBM boundary condition for PCM

The perspective of the SLI can be traced by updating the liquid fraction Eq. (32), or the no-velocity condition and total enthalpy on the acting interface are dealt with immersed boundary condition. The no-slip condition is employed in the SLI, and the evolution of Eq. (18) is only executed at the melted regime. The no-slip/bounce-back boundary condition on the SLI dealt with immersed moving boundary condition initially suggested by Noble and Torczynski [108]. The benefit of this technique is that an integrated evolution equation of the density DF is implemented on the entire domain.

Similarly, Cook et al. [109], Strack and Cook [110], and Wang et al. [111] have successfully implemented this technique to analyze particle–fluid systems. The immersed moving boundary condition is used to analyze the moving phase interface for PCMs. In this method, the evolution equation for the density DF, Eq. (15), can be updated as

$$p_i(\mathbf{x} + \mathbf{c}_i\Delta t, t + \Delta t) = p_i(\mathbf{x}, t) - \omega_p(1 - B)[f_i^c(\mathbf{x}, t) - p_i^{eq}(\mathbf{x}, t)] + \Omega_i^s + \Delta t F_i \tag{41}$$

where B is the weighting factor associated with fluid fraction and Ω is the dimensionless relaxation parameter or extra collision term and can be written as,

$$B = \frac{(1 - f_i)(\omega_f - 0.5)}{f_i + \omega_f - 0.5} \tag{42}$$

$$\Omega_i^s = p_f^c(\mathbf{x}, t) - p_i(\mathbf{x}, t) + p_i^{eq}(\rho, \mathbf{u}_s) - p_i^{eq}(\rho, \mathbf{u}) \tag{43}$$

\mathbf{u} and \mathbf{u}_s are the macroscopic velocity and solid velocity, respectively. The boundary condition for flow and thermal field of LBM can be obtained from [78, 112–114].

Thermo-physical properties of PCM

The thermo-physical properties of some common PCM and solid nanoadditives in PCM as NePCM used in the present work are illustrated in Tables 1 and 2.

Numerical modeling of PCM and NePCM

LBM Studies of PCM

In this section, the literature covering the heat transfer for phase change materials in cavities/enclosures by LBM is discussed herein in tabular form (Table 3).

Luo et al. [24] analyzed LB simulation for convection melting within the complex heat storage system occupied with PCMs for various Ra and Stefan numbers (*St*). The numerical consequences showed that the transient PCP depends on the geometrical and thermal parameters. Huang et al. [69] simulated the new LBM model for solid–liquid PCM for various Rayleigh numbers (*Ra*). Comparisons between the present results with the previous study demonstrate the feasibility and accuracy of the current approach concluded from the study. Later, Kebriti and Moqtaderi [70] examined convective solid–liquid phase change by employing LBM for various power-law indexes (*n*) and *Ra*. Results showed that as *n* augments flow at a specified Ra, the mean Nusselt number (\overline{Nu}) at the heated wall and the melting rate diminish. Sadehi et al. [115] investigated a numerical

Table 1 Thermo-physical properties of PCM

Thermo-physical properties	Paraffin Wax	Ice water	Octadecane	Galium	Lauric acid
Thermal conductivity ($W m^{-1} K^{-1}$)	0.21 if $T < T_{solidus}$ 0.12 if $T > T_{liquidus}$	0.54–0.65 (ice) 0.6 (water)	0.152–0.358	40.6	0.15–0.17
Solidus temperature (K)	319	273	300	303	315–316
Liquidus temperature (K)	321	373	300	2477	570–575
Specific heat ($J kg^{-1} K^{-1}$)	2890	2093 (ice) 4186 (water)	2150–2185	0.37	1760– 2810
Latent heat of fusion ($J kg^{-1}$)	173,400	334,000	189,000	5.59 kJ/mol	1600– 2108
Dynamic viscosity ($Ns m^{-2}$)	$0.001 \exp\left(-4.25 + \frac{1790}{T}\right)$	$8.90 * 10^{-3} - 8.90 * 10^{-4}$	0.0085	0.390 ± 0.003 mPa.s	7.30 mPa.s
Density ($kg m^{-3}$)	$\frac{750}{0.001(T-319.15)+1}$	917 (ice) 1000 (water)	774–814	5904	862–1007

Table 2 Thermo-physical properties of nanoadditives

Thermo-physical properties	GO	Al ₂ O ₃	TiO ₂	CuO	Ag
Thermal conductivity ($W m^{-1} K^{-1}$)	5000	17.65	4.8–11.8	18.0	429
Specific heat ($J kg^{-1} K^{-1}$)	717	525	683–697	540	235
Maximum addition in NePCM (mass%)	0–15	0–10	0–15	0–20	0–5
Coefficient of thermal expansion	28.4	6.54–8.68	0.8	0.85	1.89
Density ($kg m^{-3}$)	1800	3970	3970–4050	6500	10500
Diameter of nanoparticle (nm)	<20	<50	<20	<30	<10

study on the solid–liquid phase change process of multilayer Rubitherm PCMs within a tubular heat exchanger. Employing PCMs with the lowest and highest melting temperature in the vicinity of cold and hot boundaries leads to higher amounts of liquid fraction during the process. The effects of PCMs with respect to thickness and melting temperature help to choose proper PCMs with high latent heat capacity which leads to fluctuating average temperature.

Huo and Rao [117] studied PCM-based battery thermal management at a low temperature within the vertical cavity. It was remarked that the temperature of the battery diminishes gradually, and thermal distribution can be assured with the help of the latent heat of PCMs. Moreover, lower thermal conductivity, higher LH, and more significant surrounding temperature can decelerate the solidification procedure of PCMs and maintain the battery temperature. However, at higher LH of PCMs, the temperature distribution of the battery gets non-uniform, diminishing the battery's life [138]. Fuentes et al. [118] delineated melting with convection and radiation within the participating PCM. It was observed that free convection acts an essential role in the transitional behavior of the overall HT process. The absorbed heat flux within the PCMs was more significant by 3%. On the other hand, the enhanced absorbed heat flux in PCMs has a negligible influence on the melted fraction. Liu and He [119] investigated solid–liquid phase change (SLPC) with free convection within porous media. The numerical outcomes

show that the current model is efficient and accurate for studying transient SLPC within porous media.

Ren and Chan [120] elucidated PCM melting within the system utilizing interior fins. The study concluded that employing internal fins could heighten the HT in the PCM enclosure. The PCMs melt quicker if more fins are used. On the other hand, the quantity of melted PCMs at the final state gets less when the number of fins is added to the cavity. The melting rate of PCMs rises with the length of the fins. Zhu et al. [121] delineated 2D and 3D simulations for free convection melting within the square cavity. It was remarked that the melting rate of 2D is quicker than 3D in the primary stage, but the difference shrinks afterward during melting. At higher Ra, the Nu and melting rate increase. Enhancement in breadth has a minor effect on the interface, positions, and shapes in 3D, which signifies that 3D study is essential for related study.

Subsequently, Du et al. [122] proposed melting processes of large Prandtl number (Pr) PCMs by utilizing organic PCM. It was noticed that the numerical consequences agree with the existing data acquired numerically and experimentally. Compared with the existing LBM approaches, the current technique can capture the melting interface perfectly with a small grid density. Yehya et al. [123] explored the combined numerical and experimental characterization of an impure PCM employing TLBM. The numerical and experimental results demonstrate good agreement. The approach

Table 3 LBM studies for PCM for rectangular geometries

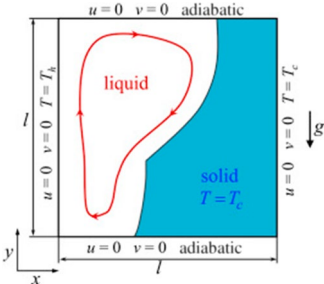
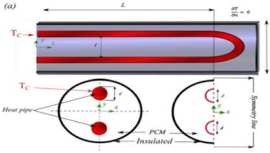
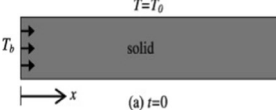
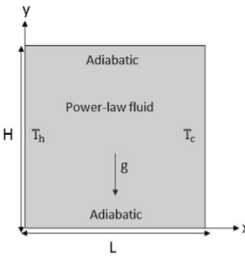
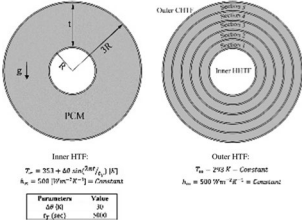
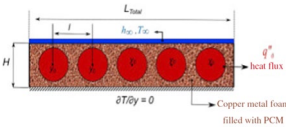
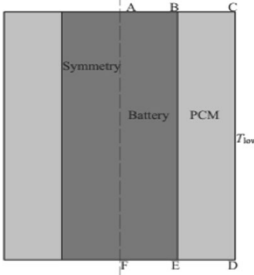
Sl No	Source	Computational domain	PCM	Model	Boundary Conditions	Parameters
1	Luo et al. [24]		Solid chemical pure substance	lattice Boltzmann models	laminar, unsteady, natural convection with no slip	$10^4 \leq Ra \leq 10^7$, $Pr = 0.1$, $St = 0.1$
2	Veismoradi et al. [57]		Paraffin Wax	Finite element method	$\frac{\partial T}{\partial x} = 0$, $\frac{\partial u}{\partial x} = 0$	$Ra = 5 \times 10^4$, $T_m = 54$
3	Huang et al. [69]		Pure substance	lattice Boltzmann models	laminar, unsteady, natural convection with no slip	$10^3 \leq Ra \leq 10^5$, $Pr = 0.02$, $St = 0.01$,
4	Kebriti and Moqtaderi [70]		Solid material	lattice Boltzmann models	laminar, unsteady, natural convection with no slip	$Ra = 5 \times 10^4$, 17×10^4 and 84×10^4 , $0.8 \leq n \leq 1.8$.
5	Sadeghi et al. [115]		Rubith-erm-31,35,42,50,58,65,70	Caramn Kozeny	Periodic time, laminar, unsteady, natural convection with no slip	$Ra = 10^6$
6	Veismoradi et al. [116]		Paraffin	Finite element method	$\frac{\partial T}{\partial x} = 0$, $\frac{\partial u}{\partial x} = 0$	$Ra = 5 \times 10^4$, $T_m = 54$
7	Huo and Rao [117]		Paraffin	lattice Boltzmann models	T_h = Isothermal (left wall) T_c = Isothermal (Right wall) Insulated top and bottom wall No slip	$Ra = 5 \times 10^4$, $T_m = 54$

Table 3 (continued)

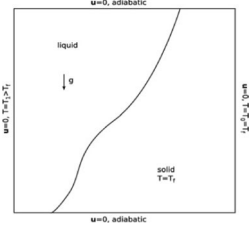
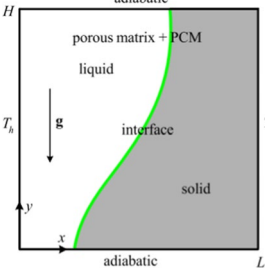
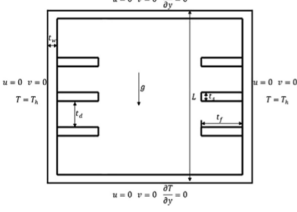
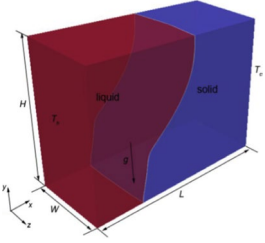
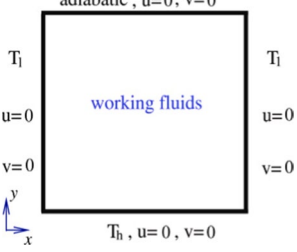
Sl No	Source	Computational domain	PCM	Model	Boundary Conditions	Parameters
8	Fuentes et al. [118]		Fatty acid	lattice Boltzmann models	T_h = Isothermal (left wall) T_c = Isothermal (Right wall) Insulated top and bottom wall No slip	21.5
9	Liu and He [119]		Isotropic and homogeneous	lattice Boltzmann models	T_h = Isothermal (left wall) T_c = Isothermal (Right wall) Insulated top and bottom wall No slip	$T_m = 29.78$, $Ra = 6.0 \times 10^5$, $Pr = 0.021$
10	Ren and Chan [120]		Fin (aluminum and steel)	lattice Boltzmann models	T_h = Isothermal (left wall) T_c = Isothermal (Right wall) Insulated top and bottom wall No slip	$Ra = 1.028 \times 10^6$, $Pr = 6.198$, $St = 0.1$, $0.1 \leq F_O \leq 0.25$
11	Zhu et al. [121]		Gallium	lattice Boltzmann models	T_h = Isothermal (left wall) T_c = Isothermal (Right wall) Insulated top and bottom wall No slip	$Ra = 6 \times 10^5$, $Pr = 0.0216$, $St = 0.039$, $T_m = 29.78$
12	Du et al. [122]		Organic material (up to $Pr = 56.2$ such as paraffin ($Pr = 56.2$), octadecane ($Pr = 56.2$))	lattice Boltzmann models	T_h = Isothermal (left wall) T_c = Isothermal (Right wall) Insulated top and bottom wall No slip	$Pr = 56.2$, $T_m = 27.6$, $10^3 \leq Ra \leq 10^5$, $St = 0.045$

Table 3 (continued)

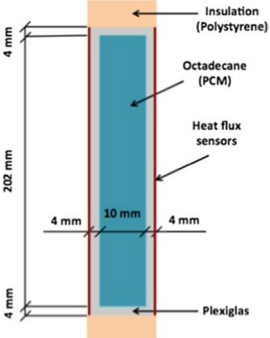
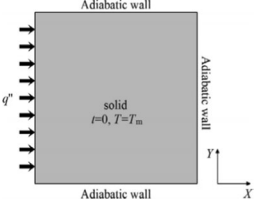
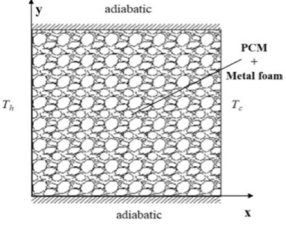
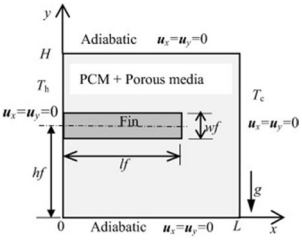


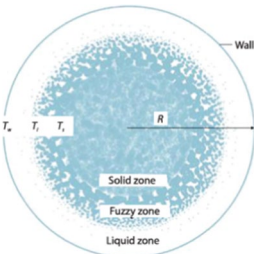
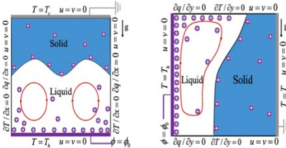
Sl No	Source	Computational domain	PCM	Model	Boundary Conditions	Parameters
13	Yehya et al. [123]		Octadecane	lattice Boltzmann models	T_h = Isothermal (left wall) T_c = Isothermal (Right wall) Insulated top and bottom wall No slip	$T_m = 27.6$, $Ra = 1.2 \times 10^4$
14	Huo and Rao [124]		Freon	lattice Boltzmann models	T_h = Isothermal (left wall) T_c = Isothermal (Right wall) Insulated top and bottom wall No slip	$Gr = 50000$, $Pr = 5$, $St = 10$
15	Huang et al. [125]		Paraffin/lauric acid	lattice Boltzmann models	T_h = Isothermal (left wall) T_c = Isothermal (Right wall) Insulated top and bottom wall No slip	$Ra = 5 \times 10^4$, $T_m = 80$, $Pr = 1$, $St = 1$, $F_0 = 0.2$
16	Gao et al. [126]		Air	lattice Boltzmann models	T_h = Isothermal (left wall) T_c = Isothermal (Right wall) Insulated top and bottom wall No slip	$Da = 1.37 \times 10^{-5}$ $St = 0.124$, $Pr = 0.020$, $\epsilon = 0.385$, $T_m = 0.391$
17	Peng and sadaghiani [127]		Paraffin	lattice Boltzmann models	T_h = Isothermal (left wall) T_c = Isothermal (Right wall) Insulated top and bottom wall No slip	$0.0 \leq \phi \leq 4.0$ $T_m = 27$
18	Ibrahim et al. [128]		Paraffin	lattice Boltzmann models	T_h = Isothermal (left wall) T_c = Isothermal (Right wall) Insulated top and bottom wall No slip	$10^3 \leq Ra \leq 10^5$, $0.0 \leq \phi \leq 2.0$, $Pr = 6.2$

Table 3 (continued)

Sl No	Source	Computational domain	PCM	Model	Boundary Conditions	Parameters
19	Lin et al. [129]		Paraffin RT35	lattice Boltzmann models	T_h = Isothermal (left wall) T_c = Isothermal (Right wall) Insulated top and bottom wall No slip	$St = 0.080,$ $0.132, 0.183$ $T_m = 18.2$
20	Jourabian et al. [130]		Ice	lattice Boltzmann models	T_h = Isothermal (left wall) T_c = Isothermal (Right wall) Insulated top and bottom wall No slip	$Pr = 6.2, Ra = 105, St = 1$
21	Gaedtke et al. [131]		Paraffin	lattice Boltzmann models	T_h = Isothermal (left wall) T_c = Isothermal (Right wall) Insulated top and bottom wall No slip	$T_m = 36$ $12 \leq F_0 \leq 51$
22	Yin et al. [132]		Solid PCM	lattice Boltzmann models	T_h = Isothermal (left wall) T_c = Isothermal (Right wall) Insulated top and bottom wall No slip	$Pr = 0.005,$ $Ra = 5 \times 10^3,$ $\epsilon = 0.1;$ and 9.34
23	Rui et al. [133]		Paraffin	lattice Boltzmann models	T_h = Isothermal (left wall) T_c = Isothermal (Right wall) Insulated top and bottom wall No slip	$Ra = 25000,$ $Pr = 0.02,$ $St = 0.5,$ $0.4 \leq F_0 \leq 1$
24	Feng et al. [134]		Composite	lattice Boltzmann models	T_h = Isothermal (left wall) T_c = Isothermal (Right wall) Insulated top and bottom wall No slip	$Ra = 2.2 \times 10^5,$ $St = 0.042,$ $Pr = 0.021,$
25	Liu et al. [135]		Paraffin	lattice Boltzmann models	T_h = Isothermal (left wall) T_c = Isothermal (Right wall) Insulated top and bottom wall No slip	$Ra = 10^6,$ $Pr = 0.02, St = 0.01,$ $F_0 = 0.36-1.08$

Table 3 (continued)

Sl No	Source	Computational domain	PCM	Model	Boundary Conditions	Parameters
26	Liu et al. [136]		Paraffin wax	lattice Boltzmann models	T_h = Isothermal (left wall) T_c = Isothermal (Right wall) Insulated top and bottom wall No slip	$10^4 \leq Ra \leq 10^6$, $Pr = 27.2, 37.2,$ and 47.2 , $St = 0.482$, $0 \leq F_0 \leq 0.0971$, $T_m = 54 \text{ }^\circ\text{C}$
27	Lu et al. [137]		Solid pure dielectric substance	lattice Boltzmann models	T_h = Isothermal (left wall) T_c = Isothermal (Right wall) Insulated top and bottom wall No slip	$2 \times 10^4 \leq Ra \leq 2 \times 10^5$, $St = 0.01$, $Pr = 0.02$, $0 \leq F_0 \leq 50$

permits highlighting the behavior of PCMs and characterizes their thermo-physical properties. Huo and Rao [124] introduced LBM for solid–liquid PCP of PCM for constant heat flux. The consequences demonstrated that additional energy on the upper part of the left wall could emphasize the clockwise rotation. Additional input energy intent in the middle of the left wall is an efficient means to speed up the solid–liquid PCP and preserve the temperature of PCMs. Huang et al. [125] explored experimentally and numerically the melting process of PCMs embedded in open-cell metal foams by using LBM. The influence of foam porosity on the HT process in porous structures is investigated. The outcome indicates that at larger porosities of the metal foams, the PCMs prove to raise the melting speed. The importance of conduction in PCMs for the melting process in metal foam is noticed.

Consequently, Gao et al. [126] presented the melting of PCM within the porous media with conducting fins. The computational outcomes showed that the melting heat transfer could be improved by adding conducting fins in the porous material. The speed of melting rises with the enhancement in the length of the fin and diminishment in the heat capacity of the fin. On the other hand, the fin in the vertical position has no significant impact on the melting rate. Peng and sadaghiani [127] elucidated the improvement of the thermal function of PCM by employing alumina nanoparticles within the circular, rectangular enclosure. The results obtained by the variation of fin numbers conclude that the more the fins, the more the MAR parameter of PCM, and later the more the improved energy storage capability. Further, the effect of the addition of

nanoparticles of Al_2O_3 into paraffin showed that 3% of nanoparticles can increase the MAR parameter rather than lower mass percentage. However, the nanoparticle concentration of more than 3% has no significant effect on the MAR parameter.

Ibrahim et al. [128] explored the effect of nanoparticles on the melting process with PCM for several pertinent parameters. It was found that the HT by conduction dominates in the initial melting phase, and then, the convection starts dominating. Also, the nanoparticles in the PCMs enhance the phase change. Besides, it was remarked that the thermal conductivity increases due to the addition of copper nanoparticles, but the melting rate and latent heat get reduced. Lin et al. [129] delineated the complex interaction of free convection and melting of PCM within a spherical capsule of various sizes. The influence of inhomogeneous PCM properties on the melting rate was nonlinear in various melting phases. Jourabian et al. [130] introduced thermal transport-free convection melting of PCMs in a partially heated square enclosure. When the heated plates are placed on top or middle of the enclosure, convection dominates in the top regime of the enclosure.

Gaedtke et al. [131] elucidated the total enthalpy-based simulation of melting in metal foam composite/paraffin PCM in 2D and 3D. The study describes the multidomain HT in 3D; the thermal conductivity of foam is 1000 times larger than paraffin. The expected sequence of the melting front and the effect of various foam-specific surface regions closely agree with the previous one. Yin et al. [132] conducted a study on SLPC at a pore scale with

central moments in TES. It was noticed that higher stability was observed at higher Ra and low viscosity. Rui et al. [133] presented free convection melting within the square enclosure. It was remarked that the top heating wall increases the melting time of the solid phase, but has a minor influence on the PC in the bottom part. The higher liquid fraction in another model was about 16.8% augmentation, and the extra top heating hastens the mean melting time by 16.8%. Feng et al. [134] explored thermal performance evaluation for bionic porous ceramic PCM utilizing micro-computed tomography. The rate of melting increases significantly due to the heat transfer path. A higher thermal contact resistance leads to lower melting time which diminishes the augmentation effect of a porous frame. Liu et al. [135] delineated solid–liquid-based phase change HT within the confined annulus. It was observed that present outcomes found excellent agreement with the previous study. Liu et al. [136] introduced a numerical study of paraffin wax melting within circular tubes for various relevant parameters. It was remarked from the study that in the SLPC process for paraffin melting, heat conduction was the primary cause in the early phase of phase transformation. The enhancement in Rayleigh number (Ra) showed the augmentation in the strength of free convection, which reduces the lessen of the \overline{Nu} due to the movement of the phase interface. Lu et al. [137] delineated HT augmentation analysis of electro-hydrodynamic (EHD) for SLPC inside a square cavity. Results showed that, during heating and injection from the lower portion, EHD rises thermal transport by modifying the onset of the flow motion within the liquid zone, whereas in the case of heating and injection from the left part, strong enough Coulomb force leads to the transition of the convection rolls which augments heat transfer at times of the melting.

Tao et al. [139] presented phase change heat transfer (HT hereafter) within metal foam or paraffin composite PCMs. The outcomes showed that the projected technique could enhance the HT process's uniformity and increase HT performance. Feng et al. [140] numerically examined the melting of nanoparticle-enhanced PCMs within the rectangular enclosure heated from the bottom portion. In the early conduction phase, melting was the dominating component in thermal transport behavior, and the melting interface was noticed.

Jourabian et al. [141] numerically studied the melting of nanoparticle-enhanced PCMs within the cylindrical tube. It was noticed that the melting point is uniform within the entire region of the cylinder at lower Ra. At the same time, it escalates at the top of the cylinder at intermediate Ra. In

addition, unstable solid flow in the lower part of the cylinder at a Ra of 10^6 leads the melting time to acute after a specific point [142]. Talati and Taghilou [143] simulated the application of LBM on the PCM solidification inside a rectangular finned container. It was noticed that the maximal time needed for freezing the PCM occurs at the aspect ratio of 0.5. Heat loss diminishes by locating the PCM within the composite plane wall. Moreover, the maximum analytical overestimation takes place at AR = 0.5.

In another study, Jourabian et al. [144] numerically studied the melting process in the porous media along two heated cylinders. The influence of thermal conductivity ratio and porosity between PCMs and porous structure is explored. It was noticed that a reduction in porosity causes a diminishment in the system melting rate and TES capacity. Moreover, augmenting the thermal conductivity proportion of the porous matrix leads to the enhancement of the melting rate. Mabrouk et al. [145] introduced the effect of porosity on the PCMs' thermal performance within the porous rectangular channel for different porosity effects under the influence of Reynold number (Re). It can be remarked from the findings that the different features of metal foam, such as porosity and conductivity, decrease later, and the augmentation in Re enhances the melting due to unsteady, forced, and laminar convection.

Han et al. [146] proposed an LBM simulation of melting heat transfer within the composite PCM. Solid–liquid interface and dynamic temperature evolution are analyzed. The consequences illustrate that the thermal performance of PCMs enhances due to metal particles as nanoparticles. Li et al. [147] numerically investigated pore-scale gravity effects on the PC HT features. It was concluded from the study that free convection acts a substantial character in the melting process. In contrast, it steadily attenuates with the diminishment in gravity, which induces the inhibiting effect of the melting process and navigates the transition of the dominant HT mechanism from convection to conduction.

Shirbani et al. [148] studied the improved TES occupying metal foam as PCMs containing several pore arrangements. It was noticed from the study that large pores could render better free convection, increasing the HT rate and decreasing the melting period. Chiappini [149] numerically studied coupled lattice Boltzmann (LB) FVM for PCM analysis. It was concluded from the study numerical, and literature data have a good agreement for the upcoming model. Ren et al. [150] presented the LBM of PCM and HT characteristics within the multilayer deposition to attain rapid prototyping and assure bonding quality. The study noticed that prediction adopts the best possible temperature state for manufacturing

and demonstrates the disparity in temperature trends at various positions.

Studies of NePCM by LBM and other traditional techniques

This present section studies the melting and solidification characteristics of NePCM in various applications with a brief description of boundary conditions and preferred models for formulation. A brief description of literature covering the heat transfer for NePCM in cavities/enclosures by LBM and other techniques is discussed herein in tabular form (Table 4).

The dispersion of hybrid nanoparticles in PCMs enclosed in a cavity with specific boundary conditions provides an enormous alteration of thermo-physical properties in the melting and solidification phase [163]. In this regard, Ghalambaz et al. [151] [164] analyzed the effect of 0–5% mass fraction Mg–MgO nanoparticles with paraffin wax in a square cavity. After melting, the thermo-physical properties were assumed to be constant; however, in the liquid phase, the hybrid nanofluids are assumed to be constant except for the density variation. A marginal variation in the liquid fraction has been observed due to the enhancement of dynamic viscosity greater than thermal conductivity enhancement. However, similar researchers analyzed the heat transfer of nanoencapsulated PCM in a porous cavity with the suspension of nanoparticles. The NePCM particles could be able to enhance the heat transfer up to 28% with a fusion temperature of 0.5 and inclination angle of 42°. However, Boukani et al. [165] analyzed the melting characteristics of NePCM in partially filled horizontal elliptical capsules with different aspect ratios and nanoparticle volume fractions. The increase in nanoparticle concentration enhances the melting rate, but decreases the NePCM volume change. It was also found that the shape of the solid–liquid interface is a function of both heat transfer rate and air void inside the capsule. To a similar extent, Selimefendigil et al. [155] analyzed the natural convection study of CuO–water nanofluid in a cavity with conductive partition and PCM under the effect of a uniform magnetic field. The results showed an average increase of heat transfer around 31.81% augmentation with a magnetic inclination of less than 5%. Chen et al. [1] elucidated a solid–liquid model for PCM melting, occupying porous media within the cylinder-shaped heat exchangers for different parameters. The

adopted technique is accepted and applied for a broad range of PCM phase changes, which promotes the design and progress of PCM heat exchangers for TES systems was noticed from the study.

However, Ghalambaz et al. [156] and Zadeh et al. [166] analyzed the thermal performance and response time of the petal-shaped shell and tube TES unit. The optimum design could improve the amount of storage capacity by 23.3% with Cu and 22.5% with GO NePCM compared to average designs. The results of this study also indicated that the geometric parameters should be considered as a primary factor in TES. In comparison, Nayak et al. [158] analyzed a free convection heat transfer in NePCM inside a circular cold cylinder with a wavy hot baffle of varying amplitude subjected to a magnetic field. The amplification of Ra accounts for the fast movement of fluid, while Ha causes the slow movement of fluid depending upon the intensity of the natural convection of NePCM. Similar results with a CFD-developed model with a heat transfer acceleration by an increasing number of baffles to 3, 7, 11, and 15 baffles provide a water temperature enhancement up to 26.37%, 29.38%, 34.06%, and 37.36%, respectively [167]. Similarly, Zidan et al. [159] analyzed the natural convection and entropy of NePCM water over a reverse T-shaped porous cavity for low emaciation of energy consumption in buildings. The use of NePCM maintains the thermal management of buildings efficiently with a better heat transfer rate. With the amplification of Ra, the intensification of streamlines, velocity fields, and structural changes of the PCM zone attained a decrease of Da. There is an uplift in Nuavg with an increase in NP concentration from 1 to 5%, which ensures an increase in heat transfer due to the addition of NPs. However, Sadeghi et al. [160] investigate natural convection and entropy generation in a NePCM-based L-shaped cavity in which St, micro-rotation, and non-dimensional fusion develop a negative impact on heat transfer and reduce Nu up to 25%, 42%, and 15%, respectively. Similar results with PCM-based heat sinks were also observed in L-shaped paraffin–copper metal foam with heat enhancement in pulse tube with steady heat flux [168]. In a similar context, Ghalambaz et al. [162] modeled a nanoencapsulated PCM in a coaxial cylindrical cavity, which ensures an unsteady charging and discharging behavior of NePCM suspension with a higher value of temperature at the particle core and an increase in heat transfer rate.

Table 4 LBM, along with other techniques studies for NePCM for geometries

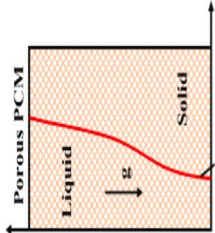
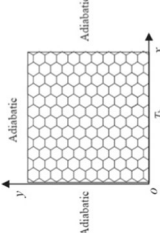
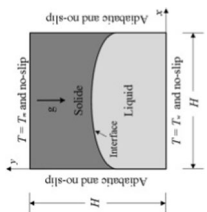
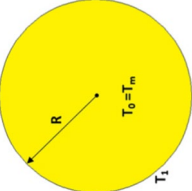
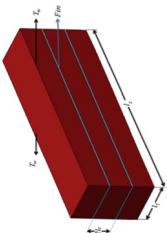
Sl No	Source	Computational domain	PCM	Model	Boundary Conditions	Parameters
1	Chen et al. [1]		Copper foam-enhanced PCM	LBM	$T_h = \text{Isothermal (left wall)}$ $T_c = \text{Isothermal (Right wall)}$ Insulated top and bottom wall No slip	$Ra = 841000$, $Pr = 0.020$, $St = 0.124$, $\epsilon = 0.385$ $T_m = 29.78$
2	Tao et al. [139]		Metal foams/paraffin composite	LBM	$T_h = \text{Isothermal (left wall)}$ $T_c = \text{Isothermal (Right wall)}$ Insulated top and bottom wall No slip	$10^6 \leq Ra \leq 10^8$, $\epsilon = 0.94 - 0.98$, $T_m = 54$
3	Feng et al. [140]		Water-copper nanoparticles	LBM	$T_h = \text{Isothermal (left wall)}$ $T_c = \text{Isothermal (Right wall)}$ Insulated top and bottom wall No slip	$Gr = 2.5 \times 10^5$, $Pr = 0.021$, $St = 0.042$, $Ra = 2.2 \times 10^5$, $AR = 1$.
4	Jourabian et al. [141]		Copper particles and water-based nanoparticles	LBM	$T_h = \text{Isothermal (left wall)}$ $T_c = \text{Isothermal (Right wall)}$ Insulated top and bottom wall No slip	$10^4 \leq Ra \leq 10^6$, $\phi = 0.04$, $Pr = 1$, $St = 10$
5	Talati and Taghilou [143]		Paraffin, aluminum, and copper	LBM	$T_h = \text{Isothermal (left wall)}$ $T_c = \text{Isothermal (Right wall)}$ Insulated top and bottom wall No slip	$AR = 0.5$, $T_m = 2.5$ and 600

Table 4 (continued)

Sl No	Source	Computational domain	PCM	Model	Boundary Conditions	Parameters
6	Jourabian et al. [144]		Water and Ni-steel porous matrix	LBM	$T_h = \text{Isothermal (left wall)}$ $T_c = \text{Isothermal (Right wall)}$ Insulated top and bottom wall No slip	$10^5 \leq Ra \leq 10^7$, $Pr = 1$ $\epsilon = 0.4$, $Da = 10^{-4}$
7	Mabrouk et al. [145]		Paraffin-saturated metal foam	LBM	$T_h = \text{Isothermal (left wall)}$ $T_c = \text{Isothermal (Right wall)}$ Insulated top and bottom wall No slip	$0.5 \leq \epsilon \leq 0.9$ $T_m = 42$, $Re = 200, 400$, $Pr = 50$
8	Han et al. [146]		Paraffin/aluminum composite	LBM	$T_h = \text{Isothermal (left wall)}$ $T_c = \text{Isothermal (right wall)}$ Insulated top and bottom wall No slip	$Ra = 5 \times 10^4, Pr = 5.2$, $St = 0.82$.
9	Li et al. [147]		Metal foams	LBM	$T_h = \text{Isothermal (left wall)}$ $T_c = \text{Isothermal (Right wall)}$ Insulated top and bottom wall No slip	$Ra = 25000$, $\epsilon = 0.9, 0.94, Pr = 0.02$, and 1 $St = 0.01$
10	Shirbani et al. [148]		Metal foam and Paraffin wax	LBM	$T_h = \text{Isothermal (left wall)}$ $T_c = \text{Isothermal (Right wall)}$ Insulated top and bottom wall No slip	$Ra = 10^5$, $Pr = 1$, $St = 0.2$
11	Chiappini [149]		Copper	LBM	$T_h = \text{Isothermal (left wall)}$ $T_c = \text{Isothermal (Right wall)}$ Insulated top and bottom wall No slip	$2 \times 10^3 \leq Ra \leq 2 \times 10^4$, $St = 4, F_0 = 0.25, Pr = 0.02$, $T_m = 37^\circ C$

Table 4 (continued)

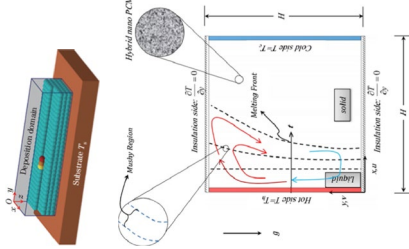
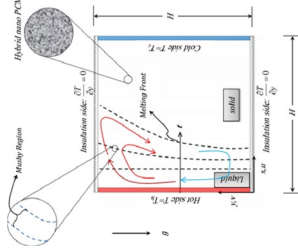
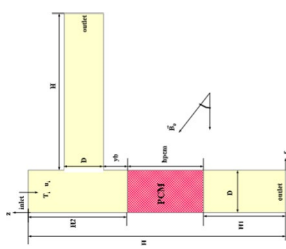
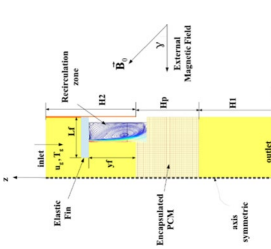
Sl No	Source	Computational domain	PCM	Model	Boundary Conditions	Parameters
12	Ren et al. [150]		Metal droplets	LBM	T_h = Isothermal (left wall) T_c = Isothermal (Right wall) Insulated top and bottom wall No slip $T_h = 40\text{ }^\circ\text{C}$ (left wall) $T_c = 30\text{ }^\circ\text{C}$ (Right wall) Insulated top and bottom wall No slip	$Ra = 2.4 \times 10^2$
13	Ghalebaz et al. [151]		0–5% Mg-MgO with paraffin	Enthalpy–porosity model	$T_h = 40\text{ }^\circ\text{C}$ (left wall) $T_c = 30\text{ }^\circ\text{C}$ (Right wall) Insulated top and bottom wall No slip	$Ra = 10^8$ $Pr = 50$ $Ste = 0.1$
14	Selimefendigi and Oztop [152]		Hybrid nanofluids (40% ethylene glycol with 60% $TiO_2-Al_2O_3$) in paraffin wax	Kozeny–Carmen permeability model	T_h = Isothermal (left wall) T_c = Isothermal (Right wall) Insulated top and bottom wall No slip	$Re = 200,500$ $Ha = 0-15$ $Yb = 0.1-0.3\text{ H2}$ $T_m = 60\text{ }^\circ\text{C}$
15	Selimefendigi and Oztop [153]		Elastic fin with water–Ag–MgO hybrid nanofluid and paraffin wax	Kozeny–Carmen permeability model	T_h = Isothermal (left wall) T_c = Isothermal (Right wall) Insulated top and bottom wall No slip	$Re = 100-700$ $E_{fin} = 10^4-10^9$ $Ha = 0-100$ $L = 0.1-0.6\text{ H2}$

Table 4 (continued)

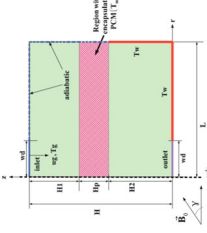
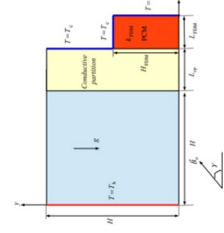
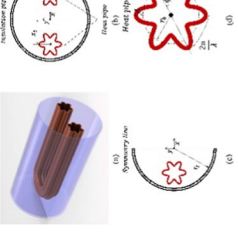
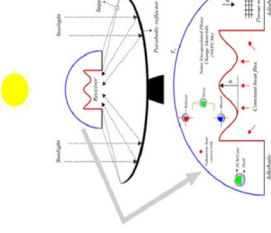
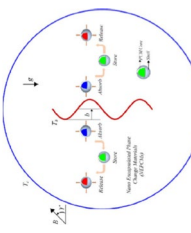
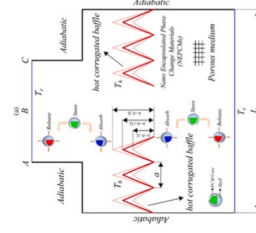
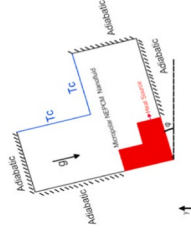
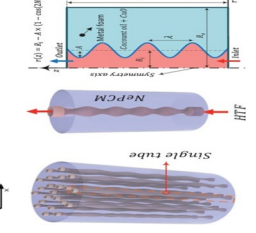
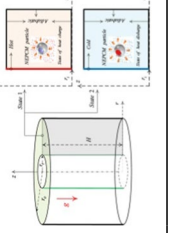
Sl No	Source	Computational domain	PCM	Model	Boundary Conditions	Parameters
16	Selimefendigil and Oztop [154]		Sphere-shaped encapsulated PCM with TiO ₂ -Al ₂ O ₃ and polyethylene glycol	Kozeny–Carmen permeability model	T_h = Isothermal (left wall) T_c = Isothermal (Right wall) Insulated top and bottom wall No slip	$Re = 250-750$ $Ha = 0-100$ $B = 0.15-0.85H$ $\alpha = 0.02-0.1\%$
17	Selimefendigil et al. [155]		CuO–water	Finite element method	$u = v = 0$ $T = T_h$ (Left) $T = T_c$ (Right) Top and bottom wall insulated	$Ra = 10^5-10^6$ $Ha = 0-100$ $H = 0.2-0.8H$ $L = 0.1-0.8H$ $K_d/K_f = 0.1-100$ $\theta = 0-0.04$
18	Ghalambaz et al. [156]		GO and Cu with paraffin wax	Finite element method with Taguchi approach	$T_h = 42\text{ }^\circ\text{C}$ $T_c = 22\text{ }^\circ\text{C}$ $T_f = 32\text{ }^\circ\text{C}$ Isothermal No slip Insulated chamber	$0.375r_s < x_{i0} < 0.625r_s$ $0 < A < 0.15t_s$ $2 < \lambda < 8$ $0 < \omega_{sl} < 8$
19	Afshar et al. [157]		CuO–water	Finite element method	$\epsilon = 0$ (all wall) $\theta = 0$ (cold wall)	$Ra = 10^3-10^5$ $Da = 10^{-1}-10^{-3}$

Table 4 (continued)

Sl No	Source	Computational domain	PCM	Model	Boundary Conditions	Parameters
20	Nayak et al. [158]		Nanoencapsulated PCM	Finite element method	$\xi=0$ (all wall) $\theta=1$ (baffle) $\theta=0$ (cylinder)	$Ra=10^3-10^5$ $\theta_f=0.05-0.95$ $Ha=0-20$
21	Zidan et al. [159]		Nanoencapsulated PCM	Finite element method with Forchheimer–Brinkman extended Darcy model	$U, V=0$ on all walls $\theta=1$ (baffles) $\theta=0$ (bottom, top wall)	$Ra=10^4-10^6$ $\xi=0.4-0.8$ $Da=10^{-4}-10^{-2}$ $\beta=0-5\%$
22	Sadeghi et al. [160]		Nanoencapsulated PCM	Finite element method	Incompressible, laminar, steady, and No slip $u=v=0$ $T=T_h$ (Left) $T=T_c$ (Right) Top and bottom wall insulated	$Ra=10^4-10^6$ $Ste=0.1-0.5$ $T_f=0.1-0.3$
23	Ghalambaz et al. [161]		Nanoencapsulated PCM	Enthalpy–porosity model	Incompressible, laminar, steady, and No slip $u=v=0$ $T=T_h$ (Left) $T=T_c$ (Right) Top and bottom wall insulated	$Ra=10^4-10^6$
24	Ghalambaz et al. [162]		Nanoencapsulated PCM	Enthalpy–porosity model	Incompressible, laminar, steady, and No slip	$Ra=10^4-10^6$ $Ste=0.2-0.4$ $\theta_f=0.1-0.3$ $\alpha=0-0.05$

Conclusions

This manuscript is proposed to assess the recent studies of PCMs for TES and heat transfer applications in fusion with LBM. In recent years, PCM has been recommended as a potential TES medium and receiving significant attention. LBM has evolved as a potential tool to solve problems based on fluid flow, thermal, multiphase, PCM, species transport, and many more studies. Most studies revealed that paraffin wax had been used as PCM for TES. A few studies have considered polyethylene glycol, lauric acid, and palmitic acid as PCM for TES. The literature associated with PCM for TES by LBM and other traditional techniques has been reviewed. TES is considered mainly from the theoretical point of view, considering various traditional techniques. The LHTES method via PCMs is an efficient means of TES and possesses the benefits of high-energy storage. The outcomes associated with various studies revealed pragmatic significance in an extensive range. PCM can be considered a future-generation energy source to encounter the increasing demand of energy sources such as solar thermal energy storage, air-conditioning unit, refrigeration system, electronic cooling, drug delivery unit, and crystal growth.

However, over the few years, the evolution of the particle-based discrete simulation method (LBM) has provided a robust and flexible approach to melting and solidification characteristics of PCM for various TES and heat transfer applications. This method develops a solid–liquid phase change model to simulate the transient phase change in porous media. It also combines an axisymmetric enthalpy change scheme to simulate the phase change efficiently by providing an elementary volume for modeling the PCM. Moreover, LBM coupled with single-relaxation and multirelaxation time schemes helps to simulate the fluid flow and temperature field. This new model is also applicable to predict the performance in various TES with brief ideas of heat transfer under various external forces. The approach is about enhancing the thermal transport area and augmenting the thermal conductivity of PCM simultaneously. Therefore, it is advised that future research focuses on the use of extended surfaces (fins, heat pipes), as well as the addition of high-conductivity materials, to improve heat transfer in LHTES systems. The authors proposed that more examination with visualization is needed to analyze the substantial augmentation in PCM for TES applications so that the changing of phase, such as the melting or solidification patterns within the PCM systems, can be characterized.

References

- Chen D, Riaz A, Aute VC, Radermacher R. A solid–liquid model based on lattice Boltzmann method for phase change material melting with porous media in cylindrical heat exchangers. *Appl Therm Eng.* 2022;207: 118080.
- Zalba B, Marin JM, Cabeza LF, Mehling H. Review on thermal energy storage with phase change: materials, heat transfer analysis and applications. *Appl Therm Eng.* 2003;23(3):251–83.
- Sharma A, Tyagi VV, Chen CR, Buddhi D. Review on thermal energy storage with phase change materials and applications. *Renew Sustain Energy Rev.* 2009;13(2):318–45.
- Liu C, Rao Z, Zhao J, Huo Y, Li Y. Review on nanoencapsulated phase change materials: preparation, characterization and heat transfer enhancement. *Nano Energy.* 2015;13:814–26.
- Henze RH, Humphrey JA. Enhanced heat conduction in phase-change thermal energy storage devices. *Int J Heat Mass Transf.* 1981;24(3):459–74.
- Yang T, King WP, Miljkovic N. Phase change material-based thermal energy storage. *Cell Rep Physcal Sci.* 2021;2(8): 100540.
- Chen D, Riaz A, Aute VC, Radermacher R. A Lattice Boltzmann model for phase change material (PCM) melting with porous media in heat exchanger; 2021
- Zhou D, Zhao C. Experimental investigations on heat transfer in phase change materials (PCMs) embedded in porous materials. *Appl Therm Eng.* 2011;31(5):970–7.
- Tian Y, Zhao C-Y. A numerical investigation of heat transfer in phase change materials (PCMs) embedded in porous metals. *Energy.* 2011;36(9):5539–46.
- Zhang S, Feng D, Shi L, Wang L, Jin Y, Tian L, et al. A review of phase change heat transfer in shape-stabilized phase change materials (ss-PCMs) based on porous supports for thermal energy storage. *Renew Sustain Energy Rev.* 2021;135: 110127.
- Tao Y, He Y-L. A review of phase change material and performance enhancement method for latent heat storage system. *Renew Sustain Energy Rev.* 2018;93:245–59.
- Lai W-C, Fan R-W. Enhanced thermal performance of form-stable phase change materials with organic and inorganic supporting nanofillers. *J Therm Anal Calorim.* 2022;147(24):14287–95.
- Kumar R, Nirwan A, Mondal B, Kumar R, Dixit A. Study on thermophysical properties of pentadecane and its composites with thermally expanded graphite as shape-stabilized phase change materials. *J Therm Anal Calorim.* 2022:1–9.
- Kumar N, Gupta SK, Sharma VK. Application of phase change material for thermal energy storage: an overview of recent advances. *Mater Today Proc.* 2021;44:368–75.
- Faraji H, Benkaddour A, Oudaoui K, El Alami M, Faraji M. Emerging applications of phase change materials: a concise review of recent advances. *Heat Transf.* 2021;50(2):1443–93.
- Liu C, Xu D, Weng J, Zhou S, Li W, Wan Y, et al. Phase change materials application in battery thermal management system: a review. *Materials.* 2020;13(20):4622.
- Zhi M, Fan R, Yang X, Zheng L, Yue S, Liu Q, et al. Recent research progress on phase change materials for thermal management of lithium-ion batteries. *J Energy Storage.* 2022;45: 103694.
- Yi F, Jiaqiang E, Zhang B, Zuo H, Wei K, Chen J, et al. Effects analysis on heat dissipation characteristics of lithium-ion battery thermal management system under the synergism of phase change material and liquid cooling method. *Renew Energy.* 2022;181:472–89.
- Wang S, Liu H, Wu D, Wang X. Temperature and pH dual-stimuli-responsive phase-change microcapsules for multipurpose applications in smart drug delivery. *J Colloid Interface Sci.* 2021;583:470–86.

20. Syah R, Davarpanah A, Elveny M, Ramdan D. Natural convection of water and nano-emulsion phase change material inside a square enclosure to cool the electronic components. *Int J Energy Res.* 2022;46(3):2403–17.
21. Selvnes H, Allouche Y, Hafner A, Schlemminger C, Tolstorebrov I. Cold thermal energy storage for industrial CO₂ refrigeration systems using phase change material: an experimental study. *Appl Therm Eng.* 2022;212: 118543.
22. Shree V, Goyal N, Saxena A, Bhattacharyya S, Dwivedi A, Goel V. Assessment of thermal loading in energy-efficient buildings: parametric review on the window design aspects. *J Therm Anal Calorim.* 2022:1–16
23. Science Wo. Number of research article published in double-diffusive convection 2022, August. <https://www.webofscience.com/wos/woscc/summary/1c278a7e-e4ca-43c2-b658-b13f21668404-258ff7e9/relevance/1>.
24. Luo K, Yao F-J, Yi H-L, Tan H-P. Lattice Boltzmann simulation of convection melting in complex heat storage systems filled with phase change materials. *Appl Therm Eng.* 2015;86:238–50.
25. Farid MM, Khudhair AM, Razack SAK, Al-Hallaj S. A review on phase change energy storage: materials and applications. *Energy Convers Manage.* 2004;45(9–10):1597–615.
26. Hoseinzadeh S, Ghasemiasl R, Havaei D, Chamkha A. Numerical investigation of rectangular thermal energy storage units with multiple phase change materials. *J Mol Liq.* 2018;271:655–60.
27. Agyenim F, Hewitt N, Eames P, Smyth M. A review of materials, heat transfer and phase change problem formulation for latent heat thermal energy storage systems (LHTESS). *Renew Sustain Energy Rev.* 2010;14(2):615–28.
28. Kurnia JC, Sasmito AP, Jangam SV, Mujumdar AS. Improved design for heat transfer performance of a novel phase change material (PCM) thermal energy storage (TES). *Appl Therm Eng.* 2013;50(1):896–907.
29. Hawlader M, Uddin M, Zhu H. Encapsulated phase change materials for thermal energy storage: experiments and simulation. *Int J Energy Res.* 2002;26(2):159–71.
30. Rathod MK, Banerjee J. Thermal stability of phase change materials used in latent heat energy storage systems: a review. *Renew Sustain Energy Rev.* 2013;18:246–58.
31. Liu S, Li Y, Zhang Y. Mathematical solutions and numerical models employed for the investigations of PCMs' phase transformations. *Renew Sustain Energy Rev.* 2014;33:659–74.
32. Liu M, Saman W, Bruno F. Validation of a mathematical model for encapsulated phase change material flat slabs for cooling applications. *Appl Therm Eng.* 2011;31(14–15):2340–7.
33. Gong Z-X, Mujumdar AS. Finite-element analysis of cyclic heat transfer in a shell-and-tube latent heat energy storage exchanger. *Appl Therm Eng.* 1997;17(6):583–91.
34. Costa M, Buddhi D, Oliva A. Numerical simulation of a latent heat thermal energy storage system with enhanced heat conduction. *Energy Convers Manage.* 1998;39(3–4):319–30.
35. Wang S, Faghri A, Bergman TL. A comprehensive numerical model for melting with natural convection. *Int J Heat Mass Transf.* 2010;53(9–10):1986–2000.
36. Archibold AR, Rahman MM, Goswami DY, Stefanakos EK. Analysis of heat transfer and fluid flow during melting inside a spherical container for thermal energy storage. *Appl Therm Eng.* 2014;64(1–2):396–407.
37. Goel M, Roy SK, Sengupta S. Laminar forced convection heat transfer in microencapsulated phase change material suspensions. *Int J Heat Mass Transf.* 1994;37(4):593–604.
38. Chakraborty S, Chatterjee D. An enthalpy-based hybrid lattice-Boltzmann method for modelling solid–liquid phase transition in the presence of convective transport. *J Fluid Mech.* 2007;592:155–75.
39. Gao D, Chen Z, Shi M, Wu Z. Study on the melting process of phase change materials in metal foams using lattice Boltzmann method. *Sci China Technol Sci.* 2010;53(11):3079–87.
40. Yang L, Jin X, Zhang Y, Du K. Recent development on heat transfer and various applications of phase-change materials. *J Clean Prod.* 2021;287: 124432.
41. Pielichowska K, Pielichowski K. Phase change materials for thermal energy storage. *Prog Mater Sci.* 2014;65:67–123.
42. Safari A, Saidur R, Sulaiman F, Xu Y, Dong J. A review on supercooling of phase change materials in thermal energy storage systems. *Renew Sustain Energy Rev.* 2017;70:905–19.
43. Fan L, Khodadadi JM. Thermal conductivity enhancement of phase change materials for thermal energy storage: a review. *Renew Sustain Energy Rev.* 2011;15(1):24–46.
44. Jebasingh BE, Arasu AV. A detailed review on heat transfer rate, supercooling, thermal stability and reliability of nanoparticle dispersed organic phase change material for low-temperature applications. *Mater Today Energy.* 2020;16: 100408.
45. Faraj K, Khaled M, Faraj J, Hachem F, Castelain C. A review on phase change materials for thermal energy storage in buildings: heating and hybrid applications. *J Energy Storage.* 2021;33: 101913.
46. Ali HM, Janjua MM, Sajjad U, Yan W-M. A critical review on heat transfer augmentation of phase change materials embedded with porous materials/foams. *Int J Heat Mass Transf.* 2019;135:649–73.
47. Pavlov G, Olesen BW, editors. Building thermal energy storage-concepts and applications. 12th ROOMVENT conference; 2011
48. Abedin AH, Rosen MA. A critical review of thermochemical energy storage systems. *Open Renew Energy J.* 2011;4(1):42–6.
49. Sivasamy P, Devaraju A, Harikrishnan S. Review on heat transfer enhancement of phase change materials (PCMs). *Mater Today Proc.* 2018;5(6):14423–31.
50. Ibrahim NI, Al-Sulaiman FA, Rahman S, Yilbas BS, Sahin AZ. Heat transfer enhancement of phase change materials for thermal energy storage applications: a critical review. *Renew Sustain Energy Rev.* 2017;74:26–50.
51. Bondareva NS, Buonomo B, Manca O, Sheremet MA. Heat transfer inside cooling system based on phase change material with alumina nanoparticles. *Appl Therm Eng.* 2018;144:972–81.
52. Jeon J, Lee J-H, Seo J, Jeong S-G, Kim S. Application of PCM thermal energy storage system to reduce building energy consumption. *J Therm Anal Calorim.* 2013;111(1):279–88.
53. Hawlader M, Uddin M, Khin MM. Microencapsulated PCM thermal energy storage system. *Appl Energy.* 2003;74(1–2):195–202.
54. Muzhanje AT, Hassan M, Hassan H. Phase change material based thermal energy storage applications for air conditioning. *Appl Therm Eng.* 2022;214:118832.
55. Shi J, Qin M, Aftab W, Zou R. Flexible phase change materials for thermal energy storage. *Energy Storage Mater.* 2021;41:321–42.
56. Peng H, Wang J, Zhang X, Ma J, Shen T, Li S, et al. A review on synthesis, characterization and application of nanoencapsulated phase change materials for thermal energy storage systems. *Appl Therm Eng.* 2021;185: 116326.
57. Veismoradi A, Ghalambaz M, Shirivand H, Hajjar A, Mohamad A, Sheremet M, et al. Study of paraffin-based composite-phase change materials for a shell and tube energy storage system: a mesh adaptation approach. *Appl Therm Eng.* 2021;190: 116793.
58. Wen R, Liu Y, Yang C, Zhu X, Huang Z, Zhang X, et al. Enhanced thermal properties of stearic acid/carbonized maize straw composite phase change material for thermal energy storage in buildings. *J Energy Storage.* 2021;36: 102420.
59. Paneliya S, Khanna S, Singh AP, Patel YK, Vanpariya A, Makani NH, et al. Core shell paraffin/silica nanocomposite: a promising

- phase change material for thermal energy storage. *Renew Energy*. 2021;167:591–9.
60. Zhang N, Guo H, Xiong L, Zhang H, Chen X. Preparation and characterization of paraffin/palygorskite shape-stable composite phase change materials for thermal energy storage. *J Energy Storage*. 2021;34: 102189.
 61. Liu S, Wu H, Du Y, Lu X, Qu J. Shape-stable composite phase change materials encapsulated by bio-based balsa wood for thermal energy storage. *Sol Energy Mater Sol Cells*. 2021;230: 111187.
 62. Feldman D, Shapiro M, Banu D. Organic phase change materials for thermal energy storage. *Solar Energy Mater*. 1986;13(1):1–10.
 63. Guo W, He Z, Zhang Y, Zhang P. Thermal performance of the packed bed thermal energy storage system with encapsulated phase change material. *Renew Energy*. 2022;196:1345–56.
 64. Almendros-Ibáñez JA, Fernández-Torrijos M, Díaz-Heras M, Belmonte J, Sobrino C. A review of solar thermal energy storage in beds of particles: packed and fluidized beds. *Sol Energy*. 2019;192:193–237.
 65. Gautam A, Saini R. A review on sensible heat based packed bed solar thermal energy storage system for low temperature applications. *Sol Energy*. 2020;207:937–56.
 66. He Z, Guo W, Zhang P. Performance prediction, optimal design and operational control of thermal energy storage using artificial intelligence methods. *Renew Sustain Energy Rev*. 2022;156: 111977.
 67. Amaral C, Vicente R, Marques P, Barros-Timmons A. Phase change materials and carbon nanostructures for thermal energy storage: a literature review. *Renew Sustain Energy Rev*. 2017;79:1212–28.
 68. Lin Y, Jia Y, Alva G, Fang G. Review on thermal conductivity enhancement, thermal properties and applications of phase change materials in thermal energy storage. *Renew Sustain Energy Rev*. 2018;82:2730–42.
 69. Huang R, Wu H, Cheng P. A new lattice Boltzmann model for solid–liquid phase change. *Int J Heat Mass Transf*. 2013;59:295–301.
 70. Kebriti S, Moqtaderi H. Numerical simulation of convective non-Newtonian power-law solid-liquid phase change using the lattice Boltzmann method. *Int J Therm Sci*. 2021;159: 106574.
 71. Jourabian M, Farhadi M, Darzi AR. Simulation of natural convection melting in an inclined cavity using lattice Boltzmann method. *Sci Iran*. 2012;19(4):1066–73.
 72. McNamara GR, Zanetti G. Use of the Boltzmann equation to simulate lattice-gas automata. *Phys Rev Lett*. 1988;61(20):2332.
 73. Perumal DA, Dass AK. A Review on the development of lattice Boltzmann computation of macro fluid flows and heat transfer. *Alex Eng J*. 2015;54(4):955–71.
 74. Chen S, Doolen GD. Lattice Boltzmann method for fluid flows. *Annu Rev Fluid Mech*. 1998;30(1):329–64.
 75. Mohamad A, El-Ganaoui M, Bennacer R. Lattice Boltzmann simulation of natural convection in an open ended cavity. *Int J Therm Sci*. 2009;48(10):1870–5.
 76. Sidik NAC, Mamat R. Recent progress on lattice Boltzmann simulation of nanofluids: a review. *Int Commun Heat Mass Transfer*. 2015;66:11–22.
 77. Bohn C, Scott SA, Dennis JS, Müller C. Validation of a lattice Boltzmann model for gas–solid reactions with experiments. *J Comput Phys*. 2012;231(16):5334–50.
 78. Kumar S, Gangawane KM, Oztop HF. Applications of lattice Boltzmann method for double-diffusive convection in the cavity: a review. *Journal of Thermal Analysis and Calorimetry*. 2022:1–33.
 79. Kumar S, Gangawane KM. Double-diffusive convection in a rectangular cavity subjected to an external magnetic field with heated rectangular blockage insertion for liquid sodium–potassium alloy. *Phys Fluids*. 2022;34(2): 023604.
 80. Wang L, Liu Z, Rajamuni M. Recent progress of lattice Boltzmann method and its applications in fluid-structure interaction. *Proc Inst Mech Eng Part C J Mech Eng Sci*. 2022;09544062221077583
 81. Caiazzo A, Junk M, Rheinländer M. Comparison of analysis techniques for the lattice Boltzmann method. *Comput Math Appl*. 2009;58(5):883–97.
 82. Shan X. Simulation of Rayleigh–Bénard convection using a lattice Boltzmann method. *Phys Rev E*. 1997;55(3):2780.
 83. Alexander FJ, Chen S, Sterling J. Lattice boltzmann thermohydrodynamics. *Phys Rev E*. 1993;47(4):R2249.
 84. He X, Chen S, Doolen GD. A novel thermal model for the lattice Boltzmann method in incompressible limit. *J Comput Phys*. 1998;146(1):282–300.
 85. Guo Z, Zheng C, Shi B, Zhao T. Thermal lattice Boltzmann equation for low Mach number flows: decoupling model. *Phys Rev E*. 2007;75(3): 036704.
 86. Guo Z, Shu C. Lattice Boltzmann method and its application in engineering. Singapore: World Scientific; 2013.
 87. Mohamad A, Bennacer R, El-Ganaoui M. Double dispersion, natural convection in an open end cavity simulation via Lattice Boltzmann Method. *Int J Therm Sci*. 2010;49(10):1944–53.
 88. Nazari M, Shokri H, Mohamad A. Lattice Boltzmann simulation of natural convection in open end cavity with inclined hot wall. *Appl Math Mech*. 2015;36(4):523–40.
 89. Dixit H, Babu V. Simulation of high Rayleigh number natural convection in a square cavity using the lattice Boltzmann method. *Int J Heat Mass Transf*. 2006;49(3–4):727–39.
 90. Mohamad A. Lattice boltzmann method. Berlin: Springer; 2011.
 91. Peng Y, Shu C, Chew Y. Simplified thermal lattice Boltzmann model for incompressible thermal flows. *Phys Rev E*. 2003;68(2): 026701.
 92. Mohamad A, Kuzmin A. A critical evaluation of force term in lattice Boltzmann method, natural convection problem. *Int J Heat Mass Transf*. 2010;53(5–6):990–6.
 93. Sathiyamoorthi A, Anbalagan S. Mesoscopic analysis of heatline and massline during double-diffusive MHD natural convection in an inclined cavity. *Chin J Phys*. 2018;56(5):2155–72.
 94. Arun S, Satheesh A. Mesoscopic analysis of MHD double diffusive natural convection and entropy generation in an enclosure filled with liquid metal. *J Taiwan Inst Chem Eng*. 2019;95:155–73.
 95. Nazari M, Louhghalam L, Kayhani MH. Lattice Boltzmann simulation of double diffusive natural convection in a square cavity with a hot square obstacle. *Chin J Chem Eng*. 2015;23(1):22–30.
 96. Jiaung W-S, Ho J-R, Kuo C-P. Lattice Boltzmann method for the heat conduction problem with phase change. *Numer Heat Transf Part B Fundam*. 2001;39(2):167–87.
 97. Ibrahim A, El-Amin M, Mohammadein A, Gorla RSR. Lattice Boltzmann technique for heat transport phenomena coupled with melting process. *Heat Mass Transf*. 2017;53(1):213–21.
 98. Lane GA. Low temperature heat storage with phase change materials. *Int J Ambient Energy*. 1980;1(3):155–68.
 99. Yanadori M, Masuda T. Heat transfer study on a heat storage container with a phase change material.(Part 2. Heat transfer in the melting process in a cylindrical heat storage container). *Solar energy*. 1989;42(1):27–34.
 100. Zhao C, Dai L, Tang G, Qu Z, Li Z. Numerical study of natural convection in porous media (metals) using Lattice Boltzmann method (LBM). *Int J Heat Fluid Flow*. 2010;31(5):925–34.
 101. He Y-L, Liu Q, Li Q, Tao W-Q. Lattice Boltzmann methods for single-phase and solid-liquid phase-change heat transfer in porous media: a review. *Int J Heat Mass Transf*. 2019;129:160–97.

102. Wang C-H, Liu Z-Y, Jiang Z-Y, Zhang X-X. Double-diffusive convection in a magnetic nanofluid-filled porous medium: development and application of a nonorthogonal lattice Boltzmann model. *Phys Fluids*. 2022;34(6): 062012.
103. Fu W-S, Huang H-C, Liou W-Y. Thermal enhancement in laminar channel flow with a porous block. *Int J Heat Mass Transf*. 1996;39(10):2165–75.
104. Beckermann C, Viskanta R. Natural convection solid/liquid phase change in porous media. *Int J Heat Mass Transf*. 1988;31(1):35–46.
105. Laouer A, Al-Farhany K. Melting of nano-enhanced phase change material in a cavity heated sinusoidal from below: numerical study using lattice Boltzmann method. *Heat Transf*. 2022;51(6):5952–70.
106. Sheikholeslami M, Gorji-Bandpy M, Ganji DD. Lattice Boltzmann method for MHD natural convection heat transfer using nanofluid. *Powder Technol*. 2014;254:82–93.
107. Khademi A, Abtahi Mehrjardi SA, Said Z, Chamkha AJ (2022) Heat transfer improvement in a thermal energy storage system using auxiliary fluid instead of Nano-PCM in an inclined enclosure: a comparative study. *J Appl Comput Mech*.
108. Noble D, Torczynski J. A lattice-Boltzmann method for partially saturated computational cells. *Int J Mod Phys C*. 1998;9(08):1189–201.
109. Cook BK, Noble DR, Williams JR. A direct simulation method for particle-fluid systems. *Eng Comput*. 2004;21:151–68.
110. Strack OE, Cook BK. Three-dimensional immersed boundary conditions for moving solids in the lattice-Boltzmann method. *Int J Numer Meth Fluids*. 2007;55(2):103–25.
111. Wang L, Zhou G, Wang X, Xiong Q, Ge W. Direct numerical simulation of particle–fluid systems by combining time-driven hard-sphere model and lattice Boltzmann method. *Particuology*. 2010;8(4):379–82.
112. Chen S, Martinez D, Mei R. On boundary conditions in lattice Boltzmann methods. *Phys Fluids*. 1996;8(9):2527–36.
113. Guo Z, Zheng C, Shi B. An extrapolation method for boundary conditions in lattice Boltzmann method. *Phys Fluids*. 2002;14(6):2007–10.
114. Maier RS, Bernard RS, Grunau DW. Boundary conditions for the lattice Boltzmann method. *Phys Fluids*. 1996;8(7):1788–801.
115. Sadeghi HM, Babayan M, Chamkha A. Investigation of using multi-layer PCMs in the tubular heat exchanger with periodic heat transfer boundary condition. *Int J Heat Mass Transf*. 2020;147: 118970.
116. Veismoradi A, Modir A, Ghalambaz M, Chamkha A. A phase change/metal foam heatsink for thermal management of battery packs. *Int J Therm Sci*. 2020;157: 106514.
117. Huo Y, Rao Z. Investigation of phase change material based battery thermal management at cold temperature using lattice Boltzmann method. *Energy Convers Manage*. 2017;133:204–15.
118. Fuentes JM, Johannes K, Kuznik F, Cosnier M, Virgone J. Melting with convection and radiation in a participating phase change material. *Appl Energy*. 2013;109:454–61.
119. Liu Q, He Y-L. Double multiple-relaxation-time lattice Boltzmann model for solid–liquid phase change with natural convection in porous media. *Physica A*. 2015;438:94–106.
120. Ren Q, Chan CL. GPU accelerated numerical study of PCM melting process in an enclosure with internal fins using lattice Boltzmann method. *Int J Heat Mass Transf*. 2016;100:522–35.
121. Zhu W, Wang M, Chen H. 2D and 3D lattice Boltzmann simulation for natural convection melting. *Int J Therm Sci*. 2017;117:239–50.
122. Du W, Chen S, Wu G. A new lattice Boltzmann method for melting processes of high Prandtl number phase change materials. *J Energy Storage*. 2021;41: 103006.
123. Yehya A, Naji H, Zalewski L. Experimental and numerical characterization of an impure phase change material using a thermal lattice Boltzmann method. *Appl Therm Eng*. 2019;154:738–50.
124. Huo Y, Rao Z. Lattice Boltzmann simulation for solid–liquid phase change phenomenon of phase change material under constant heat flux. *Int J Heat Mass Transf*. 2015;86:197–206.
125. Huang X, Sun C, Chen Z, Han Y. Experimental and numerical studies on melting process of phase change materials (PCMs) embedded in open-cells metal foams. *Int J Therm Sci*. 2021;170: 107151.
126. Gao D, Chen Z, Zhang D, Chen L. Lattice Boltzmann modeling of melting of phase change materials in porous media with conducting fins. *Appl Therm Eng*. 2017;118:315–27.
127. Peng W, Sadaghiani OK. Thermal function improvement of phase-change material (PCM) using alumina nanoparticles in a circular-rectangular cavity using Lattice Boltzmann method. *J Energy Storage*. 2021;37: 102493.
128. Ibrahim AM, El-Amin MF, Sun S. Effects of nanoparticles on melting process with phase-change using the lattice Boltzmann method. *Res Phys*. 2017;7:1676–82.
129. Lin Q, Wang S, Ma Z, Wang J, Zhang T. Lattice Boltzmann simulation of flow and heat transfer evolution inside encapsulated phase change materials due to natural convection melting. *Chem Eng Sci*. 2018;189:154–64.
130. Jourabian M, Farhadi M, Darzi AAR. Convection-dominated melting of phase change material in partially heated cavity: lattice Boltzmann study. *Heat Mass Transf*. 2013;49(4):555–65.
131. Gaedtker M, Abishek S, Mead-Hunter R, King AJ, Mullins BJ, Nirschl H, et al. Total enthalpy-based lattice Boltzmann simulations of melting in paraffin/metal foam composite phase change materials. *Int J Heat Mass Transf*. 2020;155: 119870.
132. Yin M, Wang M, Huo Y, Rao Z. Simulation of solid-liquid phase change at pore scale using lattice Boltzmann method with central moments in thermal energy storage. *J Energy Storage*. 2022;49: 104116.
133. Rui Z, Li J, Ma J, Cai H, Nie B, Peng H. Comparative study on natural convection melting in square cavity using lattice Boltzmann method. *Res Phys*. 2020;18: 103274.
134. Feng G, Feng Y, Qiu L, Zhang X. Evaluation of thermal performance for bionic porous ceramic phase change material using micro-computed tomography and lattice Boltzmann method. *Int J Therm Sci*. 2022;179: 107621.
135. Liu Q, Wang X, Feng X-B, Liu F. An enthalpy-based cascaded lattice Boltzmann method for solid-liquid phase-change heat transfer. *Appl Therm Eng*. 2022;209: 118283.
136. Liu X-Y, Zhang N-D, Li X-Q, Li C, Yu P, Liang G-J, et al. Numerical simulation of paraffin melting in circular tube using lattice Boltzmann method. *Therma Sci*. 2022;26(3A):2113–23.
137. Lu C-L, Gao X-L, Wu J, Luo K, Yi H-L. Heat transfer enhancement analysis of electrohydrodynamic solid-liquid phase change via lattice Boltzmann method. *Appl Therm Eng*. 2021;194: 117112.
138. Milyani AH, Ajour MN, Alhumade HA, Abu-Hamdeh NH. Thermal management of lithium battery packs affected by phase change materials as the heat stored in the residential heating unit. *J Therm Anal Calorim*. 2022:1–19.
139. Tao Y, You Y, He Y. Lattice Boltzmann simulation on phase change heat transfer in metal foams/paraffin composite phase change material. *Appl Therm Eng*. 2016;93:476–85.
140. Feng Y, Li H, Li L, Bu L, Wang T. Numerical investigation on the melting of nanoparticle-enhanced phase change materials (NEPCM) in a bottom-heated rectangular cavity using lattice Boltzmann method. *Int J Heat Mass Transf*. 2015;81:415–25.
141. Jourabian M, Farhadi M, Sedighi K, Darzi AAR, Vazifeshenas Y. Melting of NEPCM within a cylindrical tube: numerical study

- using the lattice Boltzmann method. *Numer Heat Transf Part A Appl.* 2012;61(12):929–48.
142. Chamkha AJ, Selimefendilgil F. MHD mixed convection of nano-fluid due to an inner rotating cylinder in a 3D enclosure with a phase change material. *Int J Numer Methods Heat Fluid Flow.* 2018.
 143. Talati F, Taghilou M. Lattice Boltzmann application on the PCM solidification within a rectangular finned container. *Appl Therm Eng.* 2015;83:108–20.
 144. Jourabian M, Darzi AAR, Toghraie D, AliAkbari O. Melting process in porous media around two hot cylinders: Numerical study using the lattice Boltzmann method. *Phys A Stat Mech Appl.* 2018;509:316–35.
 145. Mabrouk R, Naji H, Dhahri H, Hammouda S, Younsi Z. Numerical investigation of porosity effect on a PCM's thermal performance in a porous rectangular channel via thermal lattice Boltzmann method. *Int Commun Heat Mass Transf.* 2020;119: 104992.
 146. Han Q, Wang H, Yu C, Zhang C. Lattice Boltzmann simulation of melting heat transfer in a composite phase change material. *Appl Therm Eng.* 2020;176: 115423.
 147. Li X, Ma T, Liu J, Zhang H, Wang Q. Pore-scale investigation of gravity effects on phase change heat transfer characteristics using lattice Boltzmann method. *Appl Energy.* 2018;222:92–103.
 148. Shirbani M, Siavashi M, Hosseini M, Bidabadi M. Improved thermal energy storage with metal foam enhanced phase change materials considering various pore arrangements: a pore-scale parallel lattice Boltzmann solution. *J Energy Storage.* 2022;52: 104744.
 149. Chiappini D. A coupled lattice Boltzmann-finite volume method for phase change material analysis. *Int J Therm Sci.* 2021;164: 106893.
 150. Ren Y, Liu Z, Pang Y, Wang X, Xu Y. Lattice Boltzmann simulation of phase change and heat transfer characteristics in the multi-layer deposition. *Appl Math Mech.* 2021;42(4):553–66.
 151. Ghalambaz M, Doostani A, Chamkha AJ, Ismael MA. Melting of nanoparticles-enhanced phase-change materials in an enclosure: effect of hybrid nanoparticles. *Int J Mech Sci.* 2017;134:85–97.
 152. Selimefendilgil F, Öztöp HF. Combined effects of bifurcation and magnetic field on the performance of phase change material installed cylinder with small inlet temperature perturbations during nanofluid convection. *Int J Heat Mass Transf.* 2022;188: 122640.
 153. Selimefendilgil F, Öztöp HF. Impacts of using an elastic fin on the phase change process under magnetic field during hybrid nanofluid convection through a PCM-packed bed system. *Int J Mech Sci.* 2022;216: 106958.
 154. Selimefendilgil F, Öztöp HF. Thermal management and performance improvement by using coupled effects of magnetic field and phase change material for hybrid nanofluid convection through a 3D vented cylindrical cavity. *Int J Heat Mass Transf.* 2022;183: 122233.
 155. Selimefendilgil F, Öztöp HF, Chamkha AJ. Natural convection in a CuO–water nanofluid filled cavity under the effect of an inclined magnetic field and phase change material (PCM) attached to its vertical wall. *J Therm Anal Calorim.* 2019;135(2):1577–94.
 156. Ghalambaz M, Mehryan S, Veismoradi A, Mahdavi M, Zahmatkesh I, Kazemi Z, et al. Melting process of the nano-enhanced phase change material (NePCM) in an optimized design of shell and tube thermal energy storage (TES): Taguchi optimization approach. *Appl Therm Eng.* 2021;193: 116945.
 157. Afshar S, Mishra S, Dogonchi AS, Karimi N, Chamkha AJ, Abulkhair H. Dissection of entropy production for the free convection of NEPCMs-filled porous wavy enclosure subject to volumetric heat source/sink. *J Taiwan Inst Chem Eng.* 2021;128:98–113.
 158. Nayak M, Dogonchi AS, Elmasry Y, Karimi N, Chamkha AJ, Alhumade H. Free convection and second law scrutiny of NEPCM suspension inside a wavy-baffle-equipped cylinder under altered Fourier theory. *J Taiwan Inst Chem Eng.* 2021;128:288–300.
 159. Zidan A, Nayak M, Karimi N, Dogonchi AS, Chamkha AJ, Hamida MBB, et al. Thermal management and natural convection flow of nano encapsulated phase change material (NEPCM)-water suspension in a reverse T-shaped porous cavity enshrining two hot corrugated baffles: a boost to renewable energy storage. *J Build Eng.* 2022;53: 104550.
 160. Sadeghi M, Chamkha AJ, Ali R, Hamida MBB, Ghodrati M, Galal AM. Hydrothermal behavior of micro-polar nano-encapsulated phase change materials (NEPCMs) in an inclined L-shaped cavity. *Case Stud Therm Engg.* 2022;35:102039.
 161. Ghalambaz M, Melaibari AA, Chamkha AJ, Younis O, Sheremet M. Phase change heat transfer and energy storage in a wavy-tube thermal storage unit filled with a nano-enhanced phase change material and metal foams. *J Energy Storage.* 2022;54: 105277.
 162. Ghalambaz M, Mehryan S, Mashoofi N, Hajjar A, Chamkha AJ, Sheremet M, et al. Free convective melting-solidification heat transfer of nano-encapsulated phase change particles suspensions inside a coaxial pipe. *Adv Powder Technol.* 2020;31(11):4470–81.
 163. Dogonchi AS, Mishra S, Karimi N, Chamkha AJ, Alhumade H. Interaction of fusion temperature on the magnetic free convection of nano-encapsulated phase change materials within two rectangular fins-equipped porous enclosure. *J Taiwan Inst Chem Eng.* 2021;124:327–40.
 164. Ghalambaz M, Chamkha AJ, Wen D. Natural convective flow and heat transfer of nano-encapsulated phase change materials (NEPCMs) in a cavity. *Int J Heat Mass Transf.* 2019;138:738–49.
 165. Boukani NH, Dadvand A, Chamkha AJ. Melting of a nano-enhanced phase change material (NePCM) in partially-filled horizontal elliptical capsules with different aspect ratios. *Int J Mech Sci.* 2018;149:164–77.
 166. Zadeh SMH, Mehryan S, Ghalambaz M, Ghodrati M, Young J, Chamkha A. Hybrid thermal performance enhancement of a circular latent heat storage system by utilizing partially filled copper foam and Cu/GO nano-additives. *Energy.* 2020;213: 118761.
 167. Al Adel Z, Bouabidi A, Chrigui M. 3D CFD simulation and experimental validation of the baffle number effect on the solar still performance. *J Thermal Anal Calorim.* 2022;1–18.
 168. Chamkha A, Veismoradi A, Ghalambaz M, Talebizadehsardari P. Phase change heat transfer in an L-shape heatsink occupied with paraffin-copper metal foam. *Appl Therm Eng.* 2020;177: 115493.

Publisher's Note Springer Nature remains neutral with regard to jurisdictional claims in published maps and institutional affiliations.

Springer Nature or its licensor (e.g. a society or other partner) holds exclusive rights to this article under a publishing agreement with the author(s) or other rightsholder(s); author self-archiving of the accepted manuscript version of this article is solely governed by the terms of such publishing agreement and applicable law.